

FACTORS AFFECTING THE MODE
OF SOLIDIFICATION OF ALLOYS
IN A CONTROLLED FREEZING SYSTEM

by

EDWARD E. HUCKE

S.B., Massachusetts Institute of Technology
(1951)

S.M., Massachusetts Institute of Technology
(1952)

SUBMITTED IN PARTIAL FULFILLMENT
OF THE REQUIREMENTS FOR THE
DEGREE OF
DOCTOR OF SCIENCE

at the

MASSACHUSETTS INSTITUTE OF TECHNOLOGY

October, 1953

Signature of Author..
Department of Metallurgy, Oct. 23, 1953

Certified by..... Thesis Supervisor

Certified by..... Thesis Supervisor

Accepted by..... Chairman, Departmental Committee
on Graduate Students

1

FACTORS AFFECTING THE MODE OF SOLIDIFICATION OF ALLOYS
IN A CONTROLLED FREEZING SYSTEM

by

Edward E. Hucke

Submitted to the Department of Metallurgy on Oct. 23, 1953,
in partial fulfillment of the requirements
for the degree of Doctor of Science.

ABSTRACT

An apparatus capable of independent control and variation of temperature gradients and solidification velocity was designed, constructed, and used to freeze highly agitated alloy melts. Liquid agitation was achieved by low frequency induction.

Conditions necessary for maintenance of plane front solidification were investigated for aluminum-zinc, aluminum-copper, and aluminum-iron alloys over a range of freezing rate and composition. Freezing rate was varied from $.45 \times 10^{-3}$ to 3×10^{-3} centimeters per second. Alloy contents ranged from 2 to 50, .5 to 10, and .04 to 2 weight percent for aluminum-zinc, aluminum-copper, and aluminum-iron, respectively.

It was observed that different solute elements have vastly different effects on the mode of solidification. Under comparable conditions .3 weight percent iron, 2

Amalgam (metal) April 6, 1954

weight percent copper, and 12 weight percent zinc caused degeneration of plane front freezing. Degeneration of plane front solidification resulted in formation of fine equi-axed grains rather than normal dendritic growth.

A theoretically derived relation, confirmed by experiment, showed that the following factors promote plane front solidification:

1. Large diffusion coefficient for the solute in the liquid.
2. Small solute concentration.
3. Large partition ratio.
4. Low freezing rate.
5. Large liquid temperature gradient.

TABLE OF CONTENTS

<u>Sec.</u> <u>No.</u>		<u>Page</u> <u>No.</u>
	Abstract	i
	List of Illustrations	vi
	List of Tables	viii
	Acknowledgements	ix
I	INTRODUCTION AND LITERATURE SURVEY	1
	A. Introductory Remarks	1
	B. Work Assuming Perfect Liquid Diffusion	2
	C. Imperfect Liquid Diffusion	2
	D. Purpose of This Work	5
II	APPARATUS	6
	A. Basic Description	6
	B. Electrical Design	6
	1. General Considerations	6
	2. Overall Circuit Design	9
	C. Furnace Design	10
	1. Crucible and Plug	10
	2. Heat Extraction and Solidification	11
	3. Auxiliary Equipment	11
	D. Thermal Design	12
	1. General	12
	2. Maintenance of Constant Heat Input	14
	a. "Pinch" effect	14
	b. Effect of Interface Position	14
	3. Maintenance of Constant Heat Ex- traction and Constant Thermal Resistance of the Plug	14
	a. Constant Heat Extraction	15
	b. Constant Thermal Resistance	16
	1. Contact Resistance Between Ingot and Plug	16
	2. Effect of Plug Diameter and Thermal Conductivity	17
	4. Summary and Presentation of Typical Thermal Data	18

<u>Sec.</u> <u>No.</u>		<u>Page</u> <u>No.</u>
III	PROCEDURE	20
	A. General	20
	B. Preparation of Melt and Contamination . .	20
	1. Charge	20
	2. Contamination from Cooling Plug . . .	20
	3. Contamination from other Sources . .	21
	C. Effect of Starting Conditions on Interface Movement	21
	D. Maintenance of Interface Close to Stirring Source	22
	E. Measurements during Solidification . . .	23
	F. Physical Tests	24
IV	RESULTS AND DISCUSSION	25
	A. General Discussion	25
	B. Solute Concentration Gradients Created by a Moving Interface	26
	C. Conditions Necessary for Plane Front Freezing	28
	1. Effect of Stirring on Plane Front Solidification	29
	a. Unstirred Condition	29
	b. "Perfect" Stirring	29
	c. Stable Systems with No Stirring .	30
	2. Comparison of Stability in Different Alloy Systems	30
	3. Structure Expected from Plane Front Solidification	32
	D. Case of Non-Plane Front Freezing	32
	1. Complete Degeneration of Plane Front. Freezing in a Stirred System	32
	2. Slight Amounts of Supercooling . . .	33
	3. Structure Expected from Plane Front Degeneration in a Stirred System . .	34

<u>Sec.</u> <u>No.</u>		<u>Page</u> <u>No.</u>
E.	Experimental Results	35
1.	Aluminum-Copper Alloys	36
a.	Macrostructure	36
b.	Microstructure	36
1.	Coarse Grained Heats	36
2.	Fine Grained Heats	37
c.	Experimental Plot	38
2.	Aluminum-Zinc Alloys	39
3.	Aluminum-Iron Alloys	39
4.	Grain Size in Unstable Heats	40
F.	Consideration of Mode of Solidification in Other Systems	41
V	CONCLUSIONS	44
VI	SUGGESTIONS FOR FUTURE WORK	46
VII	BIBLIOGRAPHY	47
VIII	APPENDIX A	57

LIST OF ILLUSTRATIONS

<u>Fig.</u> <u>No.</u>		<u>Page</u> <u>No.</u>
1.	A Schematic Representation of "Constitutional Supercooling"	58
2.	General Scheme of the Experimental Apparatus Used	59
3.	Photograph of the Crucible and Cooling Plug Assembly	60
4.	Photograph of Experimental Apparatus	61
5.	Diagram of the Basic Elements of the Apparatus	62
6.	Overall Schematic Circuit Diagram	63
7.	Schematic Representation of the Steady State Temperature Distribution in the Apparatus	64
8.	A Plot of Measured Plug Temperature versus Time Showing the Effect of Ingot-Plug Contact Resistance	65
9.	An Experimental Plot for a Typical Heat	66
10.	An Experimental Plot for a Typical Heat	67
11.	A Plot Showing Temperature Gradients in the Cooling Plug at Various Times during a Heat	68
12.	Composition Gradient at Equilibrium with a Stationary Interface	69
13.	Composition Gradient with a Moving Interface	70
14.	A Plot of Required Liquid Temperature Gradient versus Interface Velocity for the Aluminum-Copper System	71
15.	Plot of Maximum Allowable Concentration versus Interface Velocity for Three Different Solutes in Aluminum	72
16.	Macrostructure of Heat 7	73
17.	Macrostructure of Heat 21	74
18.	Microstructure of Heat 3	75

<u>Fig.</u> <u>No.</u>		<u>Page</u> <u>No.</u>
19.	Microstructure at the Top of the Controlled Solidification Zone of Heat 3	75
20.	Microstructure of Heat 19	76
21.	Experimental Stability Plot for Aluminum-Copper Heats	77
22.	Experimental Stability Plot for Aluminum-Zinc Heats	78
23.	Macrostructure of Heat 15	79
24.	Macrostructure of Heat 25	79
25.	Macrostructure of Heat 33	80
26.	Macrostructure of Heat 34	80
27.	Macrostructure of Heat 20	81
28.	Structure of a Copper Centrifugal Casting	82

LIST OF TABLES

<u>Table No.</u>		<u>Page No.</u>
I	Comparison of Maximum Allowable Solute Concentration in Various Alloy Systems	50
II	Effect of Small Concentrations of Iron on the Structure of Directionally Solidified Pure Aluminum Ingots	51
III	Definition of Symbols	52
IV	Data for Aluminum-Copper Heats -- Plane Front Solidification	53
V	Data for Aluminum-Copper Heats -- Non-Plane Front Solidification	54
VI	Data for Aluminum-Zinc Heats -- Plane Front Solidification	55
VII	Data for Aluminum-Zinc Heats -- Non-Plane Front Solidification	56

ACKNOWLEDGEMENTS

The author wishes to express his sincere appreciation to Professor Howard F. Taylor for help and counsel throughout the course of this work, and to Professor Clyde M. Adams for advice and assistance.

In addition, the author expresses his appreciation to Merton C. Flemings, Jr., for aid in design, construction and operation of the experimental equipment, to George Schmidt for illustrations and to the entire foundry staff for aid and cooperation.

I

INTRODUCTION AND LITERATURE SURVEY

A. INTRODUCTORY REMARKS

It has long been noted that pure metals and alloys have vastly different modes of solidification. Pure metals freeze with a well defined liquid-solid interface, which advances into the melt until the whole system is solid at a rate controlled by heat flow conditions. Alloys, on the other hand, in general solidify in such a manner that there is no sharp demarcation line between areas which are completely solid and areas which are completely liquid. This behavior has been termed "mushy" freezing, and its characteristics are a function of composition as well as heat flow. The mode of solidification is of vital importance to the foundryman, since it governs such factors as fluidity and microporosity.

There have been many experimental works undertaken with the aim of evaluating the factors which determine mode of solidification. However, most of these works have been conducted in systems where the pertinent variables could not be measured or independently controlled. In such systems, experimental measuring difficulties are enormous, since the factors of interest, such as linear freezing rate, heat flow, and composition vary not only with time, but also with location in the system. Most observations must therefore be made indirectly from the structure of the completely solidified casting.

Only recently has the trend been toward less complicated experimental systems. Work on such systems has been directed toward evaluation of general behavior with the hope of applying this information to the more complicated cases. Only the previous work carried out in controlled experiments is considered in the following paragraphs.

B. WORK ASSUMING PERFECT LIQUID DIFFUSION

Pond and Kessler (1) uni-directionally solidified melts of various metals and alloys under controlled temperature gradients. They observed a cellular substructure on the liquid-solid interface, and described a purely thermal mechanism to account for its presence. This mechanism was extended to explain the growth form of dendrites in both metals and alloys. Their work took no account of imperfect solute diffusion in the liquid adjacent to the interface.

C. IMPERFECT LIQUID DIFFUSION

As early as 1935, Papapetrou (2) realized from work on mineral crystals that supersaturation of the liquid adjacent to the interface is necessary for dendrite formation. Northcott (3) also recognized that a region of high solute concentration exists in the liquid adjacent to a freezing liquid-solid interface. He postulated this layer to account for some of the grain structures observed in copper alloys.

Weinburg and Chalmers (4) in controlled solidification experiments on lead showed that supercooling of the liquid was a necessary condition for the development of a fully dendritic structure. In a later work, Rutter and Chalmers (5) used the concept of "constitutional supercooling" to explain the cellular substructure ("corrugations") they obtained on decanted interfaces of impure metal melts. Their experimental system was much the same as that of Pond and Kessler and of Weinburg and Chalmers, and consisted of a long shallow bath in which uni-directional freezing took place under controlled temperature gradients.

"Constitutional supercooling" may be schematically pictured as in Figure 1. The liquid-solid interface movement creates a solute concentration build-up at the interface due to imperfect solute diffusion in the liquid. The solute distribution next to the interface may be shown in terms of a corresponding equilibrium liquidus temperature curve. When the actual temperature gradient in the liquid falls below the equilibrium liquidus curve, a portion of the liquid adjacent to the interface is supercooled and and therefore is in an unstable condition. With such a situation, certain parts of the interface can extend ahead of the rest. This mechanism was used as an explanation for the observed "corrugations" on the decanted interfaces.

When the liquid temperature does not at any point fall below the equilibrium liquidus temperature, no part of the interface can grow ahead of another part, since, in order to do so, it must enter liquid which is above its equilibrium freezing point. Hence the interface moves as a plane front.

For a system with no liquid agitation, Tiller et al (6) described quantitatively "constitutional supercooling" in terms of the pertinent variables. They expressed the criterion for plane front solidification (no "constitutional supercooling") in terms of the following equation:

$$G = \frac{Rmc_0(1-K)}{DK} \quad (1)$$

Where G = minimum liquid temperature gradient required for plane front freezing

R = interface velocity

m = slope of the phase diagram liquidus line

c_0 = bulk liquid composition

K = partition constant

D = diffusion coefficient

Winegard and Chalmers (7) have qualitatively correlated the typically observed ingot structure with the degree and variation of supercooling in the ingot. They showed diagrammatically how supercooling may cause the dendritic columnar

zone of an ingot; and how, as solidification proceeds, this structure yields an equiaxed grain structure in the central portion of the ingot.

D. PURPOSE OF THIS WORK

The purpose of this work was to investigate both experimentally and analytically the factors which determine the mode of freezing of alloys, i.e., plane front freezing versus dendritic freezing. The previous experimental work done in controlled systems has been on alloys of very low solute concentration (impure metals) with no liquid agitation. In this work the scope was expanded to include the effect of liquid stirring and sizeable solute concentrations. From the results of such an investigation, it was hoped that information could be gained which would help to interpret solidification in common castings.

In order to carry out the desired program, an apparatus was designed and constructed which would give the necessary control over the following factors for a wide range of variation of each:

1. Heat flow
2. Temperature gradients
3. Freezing velocity
4. Liquid stirring

II

APPARATUSA. BASIC DESCRIPTION

The apparatus used was designed to meet the basic criteria outlined in Section I. The general scheme of the apparatus is shown in Figure 2. Essentially, it was required that the apparatus have control over heat flow into and out of the melt, temperature gradients in the solid, rate of solidification, and stirring of the liquid metal.

Both stirring and power were produced by low frequency induction, mechanical stirring devices being found unfeasible due to materials limitations. Figures 3 and 4 show the overall design of the final apparatus and auxiliary measuring equipment. In Figure 5, the basic elements are shown schematically. Heat is supplied by an induction coil to a charge contained in an insulated crucible. The heat input is balanced by the heat abstracted by conduction through the solid ingot, which is cooled by a water spray. Both coil and spray may be moved at constant speed upwards, moving the liquid-solid interface upwards under constant heat flow and temperature gradients.

B. ELECTRICAL DESIGN1. General Considerations

In order to meet the desired condition of high liquid agitation without putting more than the required

power into the melt, an unusual electrical design was necessary. Stated simply, induction stirring depends on the square of the coil current, and for maximum stirring, maximum coil current per unit power in the melt is desired.

The power in the melt is given by the expression:

$$P = \frac{1.77 \times 10^{-6} a \sqrt{\mu \rho \zeta} (Ni)^2 F_R Y_R}{l} \quad (2)$$

where

P = power in charge, kilowatts

a = charge radius, centimeters

μ = magnetic permeability

ρ = charge resistivity, ohm.-cm.

N = number of turns in coil

i = coil current, amperes

l = coil length, centimeters

F_R = correction factor

Y_R = correction factor

A generalization for the stirring force may be written:

$$\text{Stirring force} = (\text{constant}) \frac{(Ni)^2}{l} \quad (3)$$

From equations 2 and 3, power, as well as stirring force, is proportional to $\frac{(Ni)^2}{l}$. Both N and l were fixed by the conditions discussed in Section II, part 2. The other factors in equation (2) were, in general, chosen to minimize the power input per unit current. In this way, it was possible to take advantage of the square effect of current on stirring force while minimizing power development in the charge.

The frequency chosen was 960 cycles per second because it was the lowest frequency readily available. The charge resistivity, ρ , being a property of the alloy system, could not be chosen. The remaining factors open to variation were coil radius and charge radius, which, in addition, determine F_r and Y_r when all other factors are fixed.

Thus far, only the stirring forces have been considered and not the motion caused by the forces. The stirring action is known to vary inversely as the density of the molten liquid ⁽⁸⁾ and must also be related to hydromechanical properties of the liquid as well as to the size of the container. Unfortunately, no straightforward analysis can be made showing the quantitative relation of bath motion to stirring forces and other pertinent quantities. However, a qualitative analysis of the magnetic field and induced currents in the charge indicates that the stirring pattern is similar to that shown in Figure 5. No method was devised to measure the stirring velocity. The motion, however, was so vigorous that a pressure head of approximately 5 inches of molten alloy had to be maintained in order to keep the liquid from rising out of the crucible.

The same electromagnetic forces which cause stirring also cause the so-called "pinch effect". This effect tends to decrease the charge diameter, which in turn lowers the power input at a given current and therefore disrupts steady-state conditions. A sufficient pressure head of

molten alloy combats this effect by forcing the liquid to assume the diameter of the crucible.

It is expected that the smaller the charge (or crucible) radius, the less will be the motion for a given stirring force. Several different charge radii were tried, but no visual difference in bath motion was noted. Consequently, a convenient charge radius ($a = 1.65$ centimeters) was chosen.

2. Overall Circuit Design

In addition to the electrical considerations governing coil design, coil dimensions were limited by overall design considerations. Turns per unit length were limited by a minimum necessary cooling water flow rate, and total turns limited by a maximum desirable coil length. Too long a coil was undesirable, since, during coil movement upwards, the top of the coil could not be permitted to pass the top of the liquid level. With the charge only partly in the coil, heating efficiency may be expected to drop, and steady-state heat flow disrupted. The design adopted was a coil 9.5 centimeters in diameter by 5.5 centimeters long, with a total of 13 turns.

A coil and charge assembly of the type adopted has too low an impedance to be directly connected to the commercial 960 cycle alternator used. In order to solve this problem, the circuit shown in Figure 6 was used. The movable stirring coil is connected in series with a

large, empty induction furnace, the combination being connected in parallel with a capacitor bank for power factor correction. This circuit has two distinct advantages: (1) High currents (approximately 1000 amperes) can be passed through the stirring coil without drawing appreciable current from the alternator since the large coil has a power factor very much less than one. (2) The impedance of the large coil, which is very much greater than that of the small coil, fixes the impedance of the coil branch at a value which is large enough to connect directly to a commercial alternator. The voltage required by such an impedance then falls in a range which is accurately controlled by the alternator control circuit. Precise control of power input is a primary consideration, since a delicate balance with power withdrawn must be maintained. Since resistivity of the solid state is approximately one-half that of the liquid state, the liquid-solid interface must not move through the coil if constant power is to be maintained.

C. FURNACE DESIGN

1. Crucible and Plug

A photograph of the crucible and cooling plug in position for a heat is shown in Figure 3. The crucible consists of a zirconia tube, 1.30 inches (\pm .05 inch) inside diameter by 10 inches long. Surrounding the zirconia

tube is a rammed refractory, held in place with a sixty-four millimeter (inside diameter) vycor tube. The cooling plug, shown beneath the crucible, is a wrought 2S aluminum rod, machined to 1.30 inch diameter.

The plug extends one inch into the crucible, the top inch being sanded before each heat to permit clearance for thermal expansion. Plug and crucible were fixed to the frame before each heat, and centered with respect to the water spray and heating coil. The thermocouple shown was embedded in a one-eighth inch hole immediately below the crucible and extending to the center of the ingot.

2. Heat Extraction and Solidification

The effects of thermal variables on solidification will be discussed in part C, and only mechanical design of the essential parts described here.

Heat was removed by the water spray shown in Figure 3, which was maintained a fixed distance below the coil. Both coil and spray were mounted on a threaded shaft, rotation of which caused upward movement of the coil and spray assemblies. The shaft was driven by a variable speed direct current motor through a gear reducer and set of bevel gears. Interchangeable bevel gears were used to obtain total reductions of 1800 to 1, 3600 to 1, or 5400 to 1.

3. Auxiliary Equipment

The motor, drive screw, and attached assemblies were housed in the frame shown in Figure 4. Also mounted on the

frame were:

- a. Water control valve.
- b. Water flowmeter
- c. Motor speed resistor.
- d. Electrical connections for power and motor.
- e. Holding mount for liquid-solid interface measuring rod.
- f. Coil indicator, for reading the position of the coil.

An alternating current ammeter in conjunction with a current transformer was used to obtain reproducible coil currents.

D. THERMAL DESIGN

1. General

The heat flow characteristics of the apparatus can best be described with reference to Figure 7. The coil, water spray, and liquid-solid interface are shown schematically, and the temperature distribution throughout the length is plotted for steady-state heat flow.

Consider first the condition of the water and coil stationary positions with respect to the ingot. If heat input exactly balances heat extraction, no solidification or melting can occur, although the temperature gradients shown must be present in the solid. The temperature gradients may be increased by decreasing the coil-spray distance, and adjusting power until at steady-state, the liquid-solid interface is again maintained at the original position. The

increased heat flow must increase temperature gradients, but at steady state no melting or solidification will occur.

Consider now the coil and spray moving upwards at a constant rate, u . If heat input, heat extraction, and the thermal resistance of the solidifying ingot remain constant, then the position of the liquid-solid interface must remain constant with respect to the coil, and solidification upwards is occurring at rate u . Note heat extraction must now be equal to heat input plus heat of fusion of the solidifying metal. Again, temperature gradients may be varied independently of freezing velocity by varying the coil-water spray distance and power input. Further, the temperature gradients in the solid must remain constant throughout solidification.

The thermal design of the apparatus was based on maintaining constant temperature gradients in the solid, a constant linear freezing velocity u , and maintaining the interface a constant distance behind the stirring source (induction coil). Hence, the requirements were those mentioned above:

- a. Constant heat input.
- b. Constant heat extraction and constant thermal resistance of ingot.
- c. Constant movement of water spray-coil assemblies.

These will be discussed below.

2. Maintenance of Constant Heat Input

Power to the coil may be considered constant. The power source used was a 960 cycle, 175 kilowatt motor generator set with an amphidyne control unit. Power into the charge, however, depends upon the charge geometry and resistivity as described previously. Two effects made precautions necessary to maintain heat input constant:

a. "Pinch" Effect

The strong electromagnetic field causing stirring also tended to cause "pinching" of the liquid aluminum. The field in effect tended to reduce the charge diameter within the coil, with a consequent reduction in power input. A total liquid head of approximately 5 inches was necessary to prevent this pinching.

b. Effect of Interface Position

Because of the different inductive characteristics of liquid and solid aluminum, it was found necessary to maintain the interface below the coil to maintain constant power input.

A second source of heat input may be considered to be heat of fusion. At the solidification rates used, however, the heat of fusion is completely negligible, with respect to the total power input (see Appendix A).

3. Maintenance of Constant Heat Extraction and Constant Thermal Resistance of the Plug

a. Constant Heat Extraction

Heat removal from the liquid and solid ingot may be through three possible paths: the top of the liquid, radial heat losses from the plug, and at the water spray.

Heat losses from the top of the liquid (and radial heat losses through the crucible) may be considered to be constant because of constant temperature and constant surface area. It was necessary to abandon liquid temperature measurement during solidification, however, since solid metal tended to build up on the thermocouple, adding radiating surface, and affecting the heat balance.

Radial heat losses from the cooling plug, if appreciable, would result in gradual deceleration of interface velocity during solidification. At the temperatures used, however, these heat losses were negligible, and heat flow may be considered to be essentially axial.

With the exception of heat losses from the top of the liquid, then, heat flow is entirely through the plug, cooled at the water spray. It may be presumed that a sufficiently high water flow rate will maintain the point of contact of water and ingot at essentially water temperature, and any further increase in water flow will have no effect on rate of heat removal or temperature gradients. Experimentally, no difference in interface position during trial heats was observed when water flow rate was varied from .68

to 1.8 gallons per minute. The flow rate on all subsequent heats was approximately 1.8 gallons per minute.

Heat flow, then, is entirely axial, and the temperature in the solidifying ingot must vary from the melting point at the liquid-solid interface to water temperature at the water spray (Figure 7). The temperature variation along the ingot will then be linear if the thermal resistance of the plug remains constant and is not a function of temperature. The thermal conductivity of solid aluminum varies only slightly with temperature.

b. Constant Thermal Resistance

The sole barrier to heat flow through the solid plug has been shown to be the thermal resistance of the plug itself. Affecting this thermal resistance are contact resistance between ingot and plug, thermal conductivity of ingot and plug, cross-sectional area of ingot and plug.

(1) Contact Resistance Between Ingot and Plug

Elimination of contact resistance between the melt and plug was found essential for two reasons. First, a variation of contact resistance during an individual run, due to solidification shrinkage, caused erratic interface movement. Second, variation of contact resistance from run to run prevented exact reproducibility of temperature gradients.

Before solidification of each heat was begun, and after the charge was melted, the power and coil

position was held constant until the top of the plug was melted, and the plug became an integral part of the heat.

A plot of temperature, at the base of the crucible, versus time, is given in Figure 8. Note the marked rise in temperature occurring when contact resistance is removed.

(2) Effect of Plug Diameter and Thermal Conductivity

Since heat flow was axial, freezing rate low, and plug conductivity the only barrier to heat flow, temperature gradients are expected to be constant throughout the plug and solidifying ingot if the plug and ingot have the same thermal conductivity and diameter.

Moreover, if the temperature gradients remain constant with time, the interface must move at exactly the same velocity as the coolant.

If the thermal conductivity, or cross-sectional area of the plug varies along its diameter, temperature gradients and interface velocity will not be constant. Fine porosity, unevenly distributed, was found to cause erratic interface movement, and a wrought, machined plug^{was} adopted.

If the thermal conductivity, or cross-sectional area of the solidifying metal is constant, but different from that of the plug, interface velocity is expected to be constant but different from that of the

water spray. Hence, in the more highly alloyed heats, where the thermal conductivity of the solidifying ingot was considerably less than that of the plug, interface velocity was found to be somewhat slower than water spray velocity.

On all heats of a given alloy system, the same 2S plug, 1.30 inches in diameter, was used as cooling plug. Crucible sizes varied within .05 inch, and the thermal conductivities of the alloys varied slightly. It was possible, however, in all alloys studied, to achieve a linear freezing rate, and in all but the highly alloyed heats to maintain the interface a nearly constant distance behind the coil.

4. Summary and Presentation of Typical Thermal Data

Heat flow, with the exception of constant heat losses at the top of the liquid, has been shown to be entirely axial through the plug to the water spray. Heat of fusion of solidifying metal has been shown to be constant. Rate of interface movement is then independent of total power and dependent only on rate of movement of water spray, and any change in thermal resistance of the plug that may occur during solidification. At steady-state heat flow, rate of drop of temperature at any point in the plug must be constant with time if temperature gradients are linear, and the rate of travel of the water spray with time is constant.

Figure 9 plots position of the coil-spray assembly versus time for a 1.5 percent copper heat. Note the time lag before constant interface velocity is attained. Also plotted in Figure 9, is temperature at the base of the crucible versus time. When the interface travel becomes linear, after approximately twelve minutes, the rate of temperature drop with time is constant.

Figure 10 plots similar data for an aluminum 5 percent zinc heat run at a velocity approximately six times that of the heat of Figure 9. Note the essential characteristics are the same. It was found that in the rather low alloy content ranges used for most of the work, the effect of the alloy content on the thermal conductivity was not sufficient to appreciably affect rate of interface travel.

Figure 11 shows the temperature distribution in the plug of a 1.5% copper heat at various times. Note the lines are parallel for times above twelve minutes.

III PROCEDURE

A. GENERAL

The overall procedure used was determined by the following factors;

1. Required purity of alloys.
2. Maintenance of constant interface movement, temperature gradients, and stirring pattern over a period long enough to obtain an ingot of size suitable for examination.
3. Maintenance of liquid-solid interface close to stirring source.

B. PREPARATION OF MELT AND CONTAMINATION

1. Charge

Metals used were high-purity aluminum (99.99 percent), electrolytic copper (99.92 percent) and chemical purity zinc (99.97 percent). Alloying was performed directly in the apparatus for each individual heat. Pure aluminum was melted in the crucible and the alloy added, homogenization being obtained by the induction stirring. The copper was added as master alloy, 50 percent copper - 50 percent aluminum.

2. Contamination from Cooling Plug

Before solidification, a portion of the cooling plug was melted to remove contact resistance. That portion of the plug (one-quarter to one-half inch) therefore

became an integral part of the melt.

For reasons discussed previously, a wrought 2S plug was used. Contamination of the melt from the 2S plug was prevented by running several pure aluminum "wash heats". In each "wash heat", the plug was melted to a depth of three quarters of an inch and purified by dilution with the high-purity aluminum melt. Subsequent segregation on controlled freezing further purified the top portion of the plug. The same plug was used throughout the study of a given alloy.

3. Contamination from Other Sources

7
With the exception of the zirconia crucible, the remaining possible source of contamination was the steel measuring rod. From thermal and mechanical considerations, one-sixteenth inch steel rod was found the most satisfactory interface measuring rod. Contamination was minimized in two ways: A heavy aluminum wash was applied to the rods, and the measuring rod was used as sparingly as possible, generally not more than four or five times during the course of a heat.

C. EFFECT OF STARTING CONDITIONS ON INTERFACE MOVEMENT

The equilibrium interface velocity and position with respect to the coil is expected to be independent of the thermal conditions existing at the start of solidification. Experimentally, this was found to be true. A standard procedure was adopted, however, which enabled the condition of constant interface velocity to be reached in a reasonable length of time.

Solidification was started in the following manner: Coil position was one inch above crucible bottom (measured from coil bottom). The liquid-solid interface was melted to a position corresponding to approximately the coil bottom. Power was reduced to running power, and the drive motor started. Figure 9 presents a plot of interface and coil position versus time. Note that constant interface velocity was attained after approximately 12 minutes.

D. MAINTENANCE OF INTERFACE CLOSE TO STIRRING SOURCE

The interface position with respect to the coil was fixed with a view to two opposing factors. It was desirable to have the interface as close to the coil (stirring source) as possible, but it was found extremely difficult to maintain constant interface velocity when the interface was too close to the coil field.

With constant plug size, crucible size, composition, and with constant coil-water spray distance, interface position with respect to the coil was controlled by:

1. Power
2. Thermal conductivity of solidifying ingot
3. Melting point of solidifying ingot

With the exception of the more highly alloyed heats, the power level was maintained constant, to maintain stirring force constant, and in all heats it was possible to maintain the interface at a position of between one-half

and one inch below the coil, over a sufficiently long period of time to obtain the desired ingot length.

E. MEASUREMENTS DURING SOLIDIFICATION

During meltdown, interface position was estimated from the temperature reading of a thermocouple embedded in the cooling plug at the bottom of the crucible. For each heat, the solid plug extended one inch up into the crucible. The time at which melting of the top of the plug occurred (removal of contact resistance) was determined from a nearly discontinuous rise of the thermocouple reading (Figure 8).

Coil and water spray position were fixed initially with respect to each other and also with respect to the thermocouple at the crucible bottom. They were measured at intervals throughout the heat by readings from the coil indicator scale.

Motor drive was started when the interface was close to the bottom of the coil as estimated from temperature and checked by the interface measuring rod. Interface position was measured several times at the start and completion of each heat, and temperature measured at frequent intervals throughout the heat.

As expected from axial heat flow conditions, when the interface was moving with constant velocity, the rate of

change of temperature at the crucible base was observed to be constant (Figure 9).

Power and water flow rate were measured and held constant throughout the bulk of the experimental work.

F. PHYSICAL TESTS

After each heat, the ingot and plug were removed from the crucible. The ingot was cut from the plug a distance of one inch above the thermocouple, and the plug re-used. The ingot was sectioned and one half polished for macro- and micro-graphic examination. An eighth inch thick section, three quarters of an inch below the top of the directionally frozen portion of the ingot, was used for chemical analysis. The as-cast surface of this section was removed by sanding before analysis.

A liquid sample was taken of each heat, shortly before constant velocity of interface movement was achieved. By sampling the liquid at this time, it was possible to avoid disturbing steady-state conditions later in the heat.

IV

RESULTS AND DISCUSSION

A. GENERAL DISCUSSION

Factors which affect the mode of solidification of pure metals and alloys have long been only partially understood, although recent theories of imperfect liquid diffusion have contributed much to the subject. The complexities involved in grain formation or dendrite growth are enormous, since most of the determining factors cannot be measured directly or determined from mathematical analysis in common systems. The pertinent factors include the heat flow, temperature gradients, linear solidification rate, solute distribution, and supercooling. In ordinary systems, these factors not only vary with time, but in general, vary from place to place within a given system.

The purpose of this work has been to study such a system in which the maximum number of these variables could be measured or controlled, with the idea of applying this information to systems of more general interest.

The system chosen has been described previously under Apparatus. Certain assumptions will be made in treating the problem mathematically. They are as follows:

1. Freezing takes place when the liquid-solid interface is at a vanishingly small temperature below its equilibrium freezing point.

2. The liquid temperature gradient is positive from the interface into the bulk liquid.

3. Partition equilibrium is always maintained at the liquid-solid interface, and the partition ratio does not vary with rate of freezing, temperature, or composition.

4. Increased solute concentrations lower the liquidus temperature; i.e., m is negative.

5. Solid-state diffusion of solute is insignificant.

6. Freezing of the portion of interest does not alter appreciably the concentration of the liquid.

7. The specific volume of the solid and the liquid from which it was formed are equal.

8. The diffusion constant is independent of concentration.

B. SOLUTE CONCENTRATION GRADIENTS CREATED BY A MOVING INTERFACE

When a system such as that described is held with the liquid-solid interface stationary, the composition gradients in the liquid and solid are similar to those shown in Figure 12. However, for any finite interface velocity, a finite amount of solute is rejected from the solid and must diffuse into the liquid. Since the diffusion coefficient at the interface can never become infinite, a concentration gradient must result ahead of the interface. Furthermore, the concentration of the liquid, c_0 , is fixed; therefore, the

solute concentration at the interface, c_i , must rise. Since partition equilibrium is assumed, the concentration of the solid, c_s , must rise also. Hence, just after the interface has started to move, the concentration gradient in the liquid must be similar to that shown in Figure 13.

As the interface advances, c_i will continue to rise until a steady-state condition is reached where the amount of solute rejected by the solid is just equal to the amount diffusing into the liquid. With the use of Fick's first law, the steady-state condition may be expressed by equation (4):

$$Dg = -uc_i(1-K) \quad (4)$$

where g is the solute concentration gradient in the liquid at the interface and the other quantities have their previously described meanings. Since c_i is related to c_s by the partition ratio, equation (4) may be written:

$$g = - \frac{uc_s(1-K)}{DK} \quad (5)$$

The exact form of the concentration profile cannot, in general, be calculated in a system subjected to complicated liquid stirring, but the concentration gradient at the interface, g , may be obtained from measurement of the factors on the right side of equation (5). For the special case of no liquid stirring, the steady state concentration distribution throughout the liquid has been evaluated by Tiller, et.al. (6)

C. CONDITIONS NECESSARY FOR PLANE-FRONT FREEZING

Thus far, only concentration gradients have been considered. It is the inter-relation of concentration gradient with the existing temperature gradient that determines the mode of freezing and hence the final structure.

The concentration gradient at the interface created by a moving interface can be related to the equilibrium liquidus temperature gradient, G_0 , by the slope of phase diagram:

$$G_0 = -mg \quad (6)$$

or by substitution from equation (5):

$$G_0 = \frac{-muc_s(1-K)}{DK} \quad (7)$$

The actual temperature gradient in the liquid, G , can assume any value depending on the thermal conditions imposed on the system. The condition for plane front freezing is:

$$G \geq G_0 \quad (8)$$

When this condition is fulfilled, every point in the liquid is above its freezing temperature and no part of the interface can grow ahead of another part. Equation (8) may be rewritten as follows in terms of $G_{\min.}$, the minimum liquid temperature gradient required for plane-front freezing:

$$G_{\min.} = - \frac{muc_s(1-K)}{DK} \quad (9)$$

From equation (9), it can be seen that plane-front solidification is favored by (1) low solute concentrations,

(2) an alloy system whose phase diagram shows a small slope and a large partition ratio, (3) low interface velocities, and (4) a high diffusion coefficient.

1. Effect of Stirring on Plane-Front Solidification

a. Unstirred Condition

In a quiescent melt, no segregation occurs after steady state has been reached, (6) and therefore c_s equals c_0 . Furthermore, it can be shown from a materials balance that c_s can never be greater than c_0 . Equation (9) then becomes:

$$G_{\min.} = - \frac{muc_0(1-K)}{DK} \quad (10)$$

b. "Perfect Stirring"

Perfect stirring is defined as the stirring necessary to cause the amount of segregation predicted by the phase diagram; i.e., when $c_s = Kc_0$. This condition may be approached when stirring is sufficient to yield a boundary layer of vanishingly small thickness.

Equation (9) in this case becomes:

$$G_{\min.} = - \frac{muc_0(1-K)}{D} \quad (11)$$

An important implication of this relation is that the required temperature gradient for plane-front stability does not go to zero, even with "perfect stirring". This is true because D can never be infinite; i.e., a laminar layer must always exist at the interface, and therefore, D at the interface must always take the value for molecular diffusion.

With some intermediate degree of stirring, c_s is less than c_0 , but greater than Kc_0 . It can be noted, then, that the minimum gradient required for plane-front freezing is a maximum for an unstirred melt and a minimum for perfect stirring. In Figure 14, the minimum gradient has been plotted for the aluminum-copper system against interface velocity for the extreme cases of stirring.

c. Stable Systems With No Stirring

From equation (10), it can be seen that a pure metal requires no temperature gradient to freeze as a plane front, since c_0 is zero. Alloy systems which exhibit a maximum or minimum require no temperature gradient for plane front solidification at these points, for m is then zero.

2. Comparison of Stability in Different Alloy Systems

For a given liquid temperature gradient, interface velocity, and stirring pattern, the maximum amount of solute, $(c_0)_{\max.}$, that can be tolerated without breakdown of a plane-front interface is determined by m , K and D . It is of interest to compare one alloy system with another, using values of liquid temperature gradient and interface velocity obtainable with the experimental apparatus used.

Several systems are compared in Table I for both "perfect" and no stirring. The values shown are the maximum solute concentration which can be tolerated without breakdown of plane-front freezing. For purposes of calculation, a value of $G = 150^\circ\text{C}/\text{cm}$ was used. The diffusion

constant was assumed to be 5×10^{-5} cm²/sec. when no other data were available. The interface velocity was chosen as $u = 5 \times 10^{-4}$ cm/sec.

From the tabulated values, it can be seen that different alloys affect plane front stability by vastly different amounts. In aluminum, trace amounts of iron could cause instability, while rather large alloy contents can be tolerated with zinc.

Figure 15 shows $(c_o)_{\max}$ plotted against interface velocity for both "perfect" and no stirring with a constant liquid temperature gradient of 150°C/cm. It can be noted that at higher velocities, $(c_o)_{\max}$ has a rather small value, while with decreasing velocities $(c_o)_{\max}$ increases rapidly. It can be further noted that more benefit is to be derived from stirring when K is small.

All the remarks made thus far are, in theory, universally applicable to any alloy system, providing the necessary physical constants are known. However, since very low concentrations of certain elements are quite important, some systems which are essentially binary alloys must, in actuality, be considered as ternaries. In this case, seldom are the physical constants known. This difficulty forced abandonment of work on the lead-silver system. For this system, $(c_o)_{\max}$ was of the same order as many of the trace impurities associated with the lead used.

3. Structure Expected from Plane-Front Solidification

When a melt freezes with a perfectly plane-front interface, there are no crevices to entrap liquid of high solute concentration and, therefore, the resulting ingot is homogeneous. Since no liquid is entrapped any gas evolved during freezing is free to escape. An ingot frozen with a plane front would be expected to show no microporosity. The solid composition is constant throughout the steady-state portion, rises in the initial transitory zone, and again rises when the assumption that c_0 remain constant becomes seriously in error.

The melt would be expected to solidify in long grains or even a single grain, depending on the seed crystals present at the start of solidification.

D. CASE OF NON-PLANE-FRONT FREEZING

Thus far, the discussion has not considered the case when the actual liquid temperature gradient is less than the minimum gradient required for plane-front freezing. The true temperature and liquidus temperature curves are then similar to those shown in Figure 1. Such a situation is unstable and has been described by Rutter and Chalmers (5) as "constitutional supercooling".

1. Complete Degeneration of Plane-Front Freezing in a Stirred System

It is possible for a system, which will at steady

state be unstable, to freeze as a plane front while c_i is building up to its steady-state value. When c_i reaches an unstable point, nucleation of independent grains occurs ahead of the interface, isolating a small channel of liquid from the stirring action. Growth proceeds rapidly throughout the supercooled zone, trapping areas of high solute concentration liquid between the advancing interface and the newly formed grains. Growth of these grains into the bulk liquid is retarded since they are not connected to the interface, and, therefore, heat abstraction from them is retarded. The interface eventually rejoins the newly formed grains; however, the supercooled zone has been removed since the high solute regions have been isolated from the main body of the liquid. Plane-front solidification may then continue until the solute concentration again reaches an unstable value and the process repeats itself.

2. Slight Amounts of Supercooling

"Constitutional supercooling", although an unstable condition, may actually exist without causing complete degeneration of plane-front freezing under certain conditions. (5) (9)

When no agitation is present and the degree of supercooling very small, the supercooled region may be stable due to a nucleation barrier. Under these conditions it is possible that portions of the interface extend into

the supercooled zone ahead of the main interface. Rutter and Chalmers (5) attribute the observation of "corrugations" on rapidly decanted interfaces to such conditions.

In the experimental system used, Flemings (10) has shown that the "effective thickness" of the boundary layer is about .03 centimeters. At distances slightly greater than .03 centimeter from the interface, a turbulent condition exists which offers no barrier to heterogeneous nucleation. In such a case, the supercooled zone could not extend beyond the boundary layer without nucleation occurring. There is, however, a possibility of very small "corrugations" forming when the supercooled zone is well within the boundary layer, a condition corresponding to a very slight degree of supercooling. In general, this work is concerned with amounts of supercooling sufficient to cause nucleation ahead of the interface.

3. Structure Expected from Plane Front Degeneration in a Stirred System

The preceding discussion would suggest a structure of fine grains with areas of high solute concentration appearing at intervals along the ingot, followed by a new set of randomly oriented fine grains. The average length of the grains should depend on the time required for a given alloy to reach an unstable state. It is expected, therefore, that at a given interface velocity, the grain

size should decrease with increasing c_0 .

E. EXPERIMENTAL RESULTS

Experimentally, G cannot be measured directly. Furthermore, since the temperature distribution in the boundary layer cannot be calculated for complicated systems, it is impossible to obtain G from the bulk liquid temperature. However, if the gradient in the solid, G_s , is measured, G can then be determined from the relation (See Appendix A):

$$k_1 G = k_s G_s \quad (12)$$

where k_1 and k_s are the thermal conductivities of liquid and solid respectively.

Equation (9) may then be rewritten in terms of the experimentally measured quantities.

$$\frac{(G_s)_{\min}}{c_s} = - \left[\frac{k_1 m (1-K)}{k_s DK} \right] u$$

The solid gradient was determined from the thermocouple reading (Fig. 5) and the interface temperature. As has been stated previously (Section II), this gradient was essentially linear and remained constant during all but highly alloyed heats.

When the ratio $\frac{(G_s)_{\min}}{c_s}$ is plotted against u , a straight line passing through the origin is obtained, whose slope is determined by the bracketed group of physical constants, which are presumed known.

For each of the experimental heats, the value of $\frac{G_s}{c_s}$ has been plotted against u . The value of c_s obtained from chemical analysis for the fine grained heats is an approximation since some liquid entrapment occurred in these heats. However, Flemings⁽¹⁰⁾ has shown that entrapment under these conditions affects the resulting macrosegregation only slightly.

1. Aluminum-Copper

a. Macrostructure

Each heat was sectioned and etched for macroscopic examination. Two basic structures were observed: 1. large "columnar" grains and, 2. fine grains. Figures 16 and 17 show representative views of each type structure. The section of the ingot of interest is at the bottom, and extends for approximately an inch along the ingot. The remainder of the ingot is that portion required as pressure head as previously discussed in Section II. This portion was frozen after the power was shut off and shows a typical chill cast structure. Henceforth the discussion will only be concerned with the structure of the "controlled solidification" zone at the bottom.

b. Microstructure

Representative coarse and fine grained heats were examined under the microscope.

1. Coarse grained heats

The coarse grain structure corresponded to that expected from plane front solidification. These heats showed a homogeneous solid solution with no entrapped areas of high solute concentration. Figure 18 shows an example of such a structure. Although the melt undoubtedly contained a large amount of hydrogen, no micro-porosity was found.

At the top of the controlled solidification zone a rather interesting area was observed. Here a high concentration boundary layer existed, which became unstable when the power was turned off, giving a structure very much similar to that of the fine grained heats, but with more entrapped areas. In Figure 19 areas of eutectic can be seen trapped between numerous small grains.

2. Fine grained heats

An example of the structure observed in fine grained heats is shown in Figure 20. These heats showed areas of high solute concentration (second phase) periodically spaced along the ingot and for the most part at grain boundaries. The entrapped areas were very small (approximately .002 centimeters) in size.

The observed structure gave every evidence of non-plane front solidification. This evidence was further strengthened by the similarity of the observed structure with postulated mechanism for non-plane front freezing discussed previously.

The presence of the coarse grained structure was therefore assumed to correspond to plane front freezing, and the presence of a fine grained structure was assumed to indicate degeneration of plane front conditions.

c. Experimental Plot

In Figure 21 the experimental plot of $\frac{G_s}{c_s}$ versus u is shown for the aluminum-copper heats. A straight line can be drawn between the coarse and fine grained heats. Figures 16 and 17 show the macro-structures of the two heats on either side of the line.

The slope of the experimental line differs by a factor of about 3 from the slope predicted from the physical constants. This difference may be accounted for by one or more of the following reasons:

1. The value of k_1 used was that for pure aluminum. Actually, the liquid at the interface may contain considerable solute (up to 10% copper for some of the heats). The value of k as a function of copper content is not known for either the liquid or solid states. However, from general consideration of thermal conductivity variation with composition in the solid state, it is not unreasonable to assume that k_1 may decrease by a factor of 2 or more in cases where the interface concentration was very high.

2. The diffusion coefficient may also be affected by variation in interface concentration. In

addition, its measured magnitude may be slightly in error.

3. K and m were assumed to be independent of concentration. This assumption may be slightly in error.

4. It has been assumed that instability occurs when $G = G_{\min}$. If slight amounts of supercooling were present before complete degeneration of the interface occurred, the observed value of the slope would be less than that predicted from the physical constants.

2. Aluminum-Zinc Alloys

Figure 22 shows the experimental plot of $\frac{G_s}{c_s}$ versus u for the aluminum-zinc heats. As in the case of aluminum-copper, a straight line can be drawn between the coarse and fine grained heats. Figures 23 and 24 show the macrostructures of two heats on either side of the line.

Again the observed slope differed from the calculated slope, most probably due to the same reasons discussed previously for aluminum-copper. In the case of zinc even greater deviation is to be expected due to the generally higher solute concentration at the interface (up to 40 percent).

3. Aluminum-Iron Heats

In Section IV, part 2, it was noted that the values of m , K , and D determine the maximum amount of solute that can be tolerated without degeneration of plane-

front freezing in a given freezing system. From Table I, it can be seen that the values of these constants for aluminum-copper and aluminum-zinc are quite different, but the difference in $(c_0)_{\max}$ for the two systems is not large. It was therefore of interest to investigate a system in which $(c_0)_{\max}$ is of a different order of magnitude. Aluminum-iron is such a system.

A series of aluminum-iron heats was made at approximately constant interface velocity and solid temperature gradient so that stability could be compared on the basis of c_0 .

Table II shows the value of c_0 for these heats along with their macrostructure. The observed stability limit was found to lie between .123 and .229 percent, as compared to about 1.5 percent for aluminum-copper and about 12 percent for aluminum-zinc under similar conditions. Figures 25 and 26 show the macrostructures of the two heats on either side of the stability limit.

4. Grain Size in Unstable Heats

Grain size in the fine grained heats was observed to vary considerably. At a given interface velocity, grain size was observed to decrease with increasing c_0 , as expected in light of the postulated mechanism of formation for the fine grains (see Section D, part 3 of Results and Discussion).

Figures 17 and 27 show an example of this grain size variation.

F. CONSIDERATION OF MODE OF SOLIDIFICATION IN OTHER SYSTEMS

Thus far, mode of solidification and solidification structure have been considered only under controlled experimental conditions. Factors affecting mode of solidification under common conditions are of great theoretical as well as practical interest. Several special cases will be considered here, in light of the preceding discussion.

Weinburg and Chalmers ⁽⁴⁾ and Winegard and Chalmers ⁽⁷⁾ have considered the relationship between dendrite formation and supercooling. Flemings ⁽¹⁰⁾ has shown that in many castings this supercooling must be very small, and must be related to microsegregation and structure. At the present time, however, only a qualitative approach to the mode of solidification in uncontrolled systems is possible.

Some of the concepts of imperfect liquid diffusion are helpful in explaining anomalous behavior in the mode of solidification of pure metals. It has been shown in Part 1 of Section IV that pure metals are expected to freeze with a plane front interface. A pure metal may then be described as being sufficiently low in alloy content so as plane front solidification will occur with a negligible temperature gradient in the liquid. It is of interest to consider the order of impurities that could cause a "pure" metal to freeze dendritically.

Rutter and Chalmers ⁽⁵⁾ have shown that minute impurities can cause "corrugations" to form on a liquid-solid

interface solidified at low velocities. Previous discussion has shown that very small amounts of iron in aluminum can cause degeneration of plane front freezing, even at very low velocities and with a sizable temperature gradient.

Heat transfer analysis has been used for pure metals in sand molds to predict accurately fraction solid versus time ⁽¹¹⁾. These calculations were checked experimentally by pouring out the un-solidified liquid. Good agreement was obtained with some metals, a notable exception was high purity aluminum (99.99) contaminated only by crucible pick-up. In this case, as much as 40 percent solid in excess of that calculated was observed. This discrepancy must be explained by dendritic freezing entrapping liquid so that it remained after pouring out.

A further hint of dendritic freezing in seemingly pure metal lies in the behavior of 99.90 percent copper centrifugal castings. In this case the metal was poured into a spinning tubular mold, ⁽¹²⁾ and as solidification progressed, the liquid, which was initially at rest, picked up speed until it was rotating at approximately the same speed as the solid metal. The spin was abruptly stopped after partial solidification, but the liquid, due to inertia, slowed gradually and finally came to rest at the bottom as shown in Figure 28.

Arrow A in Figure 28 indicates the direction of rotation of the mold. Arrow B indicates the initial direction

of liquid travel with respect to the solid. Note that the columnar grains tended to point in an opposite direction to the relative liquid motion, especially during the early stages of solidification when the relative liquid velocity was greatest. As the liquid gained speed the grains pointed more and more along the radius until finally they changed direction abruptly when rotation of the mold was stopped and the relative liquid velocity changed direction.

From this observation it is evident that the direction of dendrite growth depends on the direction and velocity of the liquid flow with respect to the solid. These observations can be explained in terms of imperfect liquid diffusion of small impurity elements.

Consider a dendrite arm protruding into the liquid, and rejecting impurity solute. It has been shown that this rejection of solute results in a boundary layer of higher solute concentration than the bulk liquid.

Flemings (10) has shown that the boundary layer thickness and interface solute concentration is a function of liquid agitation, and that this boundary layer acts as a barrier to growth. It is therefore expected the impinging fluid flow on the upstream side of the dendrite arm must reduce the barrier to growth on this side, and the dendrites should tend to grow upstream.

V

CONCLUSIONS

From the experimental results of this work, the following conclusions may be drawn:

1. The factors aiding attainment of a plane front solidification interface are:
 - a. Low solidification velocity
 - b. Low concentration of solute in the liquid.
 - c. Large partition ratio
 - d. High degree of stirring
 - e. Large diffusion coefficient
 - f. Large liquid temperature gradient
2. Regardless of the degree of stirring, a positive temperature gradient in the liquid is required to maintain plane front solidification in all but hyper-pure metals.
3. Plane front solidification can be experimentally maintained with alloys of sizable solute concentration; e. g., greater than 10 weight percent zinc in aluminum.
4. Degeneration of plane front freezing results in formation of fine equi-axed grains rather than normal

dendritic growth when a large positive temperature gradient is maintained in the liquid.

VI

SUGGESTIONS FOR FUTURE WORK

The experimental conditions in this work were such that degeneration of plane front solidification resulted in fine grain formation instead of the usual dendritic structure.

Future investigations of mode of solidification should be carried out under controlled conditions which would promote dendritic growth. Such an investigation should be directed toward quantitative determination of the factors governing dendrite formation.

VII

BIBLIOGRAPHY

1. Pond, R. B. and Kessler, S. B, "Model for Dendrite Growth Form in Metals and Alloys", Journal of Metals, 3, 1951, p 1156-1162.
2. Papapetrou, A., "Untersuchungen über Dendritisches Wachstum von Kristallen", Zeitschrift für Kristallographic, 92, 1935, p 89.
3. Northcott, L., "The Influence of Alloying Elements on the Crystallization of Copper. Part I - Large Additions and the Part Played by the Constitution", Journal of the Institute of Metals, 65, 1939, p 173-204.
4. Weinburg, F., and Chalmers, B., "Dendritic Growth in Lead", Canadian Journal of Physics, 29, September 1951, p 382-392.
5. Rutter, J. and Chalmers, B., "A Prismatic Substructure Formed During Solidification of Metals", Canadian Journal of Physics, 31, January 1953, p 15.
6. Tiller, W. A., Jackson, A. L., Rutter, J. W., and Chalmers, B., "The Redistribution of Solute Atoms During the Solidification of Metals", Acta Metallurgica, 1, No. 4, p 428-437.
7. Winegard, W. C and Chalmers, B., "Supercooling and Dendritic Freezing in Alloys", To be published.
8. Stansel, N. R., "Induction Heating", McGraw-Hill, Inc. (New York), 1949.

9. Wagner, C., "Theoretical Analysis of the Diffusion of Solutes During the Solidification of Alloys", To be published.
10. Flemings, M. C., "Factors Affecting Segregation in the Controlled Solidification of Aluminum-Copper and Aluminum-Zinc Alloys", Sc.D. Thesis, M.I.T., 1953.
11. Van Allstyne, P. C., "The Effect of Metal Temperature on the Thermal Properties of Foundry Molding Sand", S.M. Thesis, M.I.T., 1953.
12. Register, C. L., "Temperature Distribution in Centrifugal Casting", Sc.D. Thesis, M.I.T., 1953.

BIOGRAPHICAL NOTE

The author was born on September 1, 1930, in Kansas City, Missouri, where he received his primary and secondary school education. He entered the Massachusetts Institute of Technology in September of 1947 and has been in continuous residence there since. He received his Bachelor of Science degree in June, 1951 and his Master of Science degree in June, 1952.

The author is a member of Sigma Xi, and a member of the student chapter of the American Foundrymen's Society. In August, 1953, he published jointly a paper in The Welding Journal, entitled, "Welding Metallurgy of Nodular Cast Iron".

TABLE I

Comparison of Maximum Allowable Solute Concentration in Alloy Systems.

$$G = 150^{\circ}\text{C}/\text{cm}$$

$$u = 5 \times 10^{-4} \text{ cm}/\text{sec}$$

* Assumed value

<u>ALLOY</u>		<u>$D \times 10^5$</u>	<u>K</u>	<u>-m</u>	<u>$(c_o)_{\text{max}}$ in wt.%</u>	
Base	Solute	cm^2/sec		$^{\circ}\text{C}/\text{wt.}\%$	"Perfect" Stirring	No Stirring
Al	Cu	7.0	.171	3.38	7.50	1.28
Al	Zn	6.2	.445	1.67	20.0	8.90
Al	Fe	1.4	.018	2.94	1.46	.026
Al	Mg	2.7	.285	4.30	2.62	.748
Pb	Ag	3.6	.040	9.20	1.22	.049
Cu	Mg	5.0	.289	37.3	.566	.163
Cu	Sn	5.0	.540	11.4	2.86	1.54
Cu	Zn	5.0	.860	5.54	19.4	16.7

TABLE II

Effect of Small Concentrations of Iron on the Structure
of Directionally Solidified Pure Aluminum Ingots

$$u = 1.5 \times 10^{-3} \text{ cm/sec.}$$

$$G_s = 70^\circ\text{C./cm.}$$

HEAT NUMBER	c_o (wt.%)	STRUCTURE
30	.044	Coarse grained
31	.037	Coarse grained
32	.057	Coarse grained
33	.123	Coarse grained
34	.229	Fine grained
35	.156	Fine grained

TABLE III

Definition of Symbols

D	Diffusion coefficient
g	Solute concentration gradient in the liquid at the interface
u	Interface solidification velocity
c_i	Solute concentration in the liquid at the interface
c_o	Solute concentration in the bulk liquid
$(c_o)_{\max}$	Maximum allowable solute concentration in bulk liquid for maintenance of plane front solidification
c_s	Solute concentration in the solid
K	Partition ratio
m	Slope of the liquidus line on the phase diagram
G	Actual liquid temperature gradient at the interface
G_o	Equilibrium liquidus temperature gradient at the interface
G_s	Actual solid temperature gradient
G_{\min}	Minimum liquid temperature gradient at the interface for plane front solidification
$(G_s)_{\min}$	Minimum solid temperature gradient for plane front solidification
k_l	Thermal conductivity of the liquid in the laminar layer
k_s	Thermal conductivity of the solid

$$\left(\frac{dT_L}{dx}\right)_{x=0} = G_o \quad T_L = \text{liquidus at equilibrium}$$

TABLE IV

Data for Aluminum-Copper Heats -- Plane Front Solidification

HEAT NUMBER	C_0 (wt.%)	C_S (wt.%)	$u \times 10^3$ (cm/sec)	G_S ($^{\circ}\text{C}/\text{cm}$)	$\frac{G_S}{\sigma_S} \left(\frac{^{\circ}\text{C}}{\text{cm-wt.}\%} \right)$
1	1.02	.47	1.59	76.1	162
2	1.08	.57	1.80	66.6	117
3	1.45	.82	1.66	66.6	81.3
4	.65	.30	1.39	61.2	204
5	1.02	.30	.881	61.5	205
6	.69	.28	3.00	59.9	214
7	.98	.53	2.86	59.1	112
8	.91	.20	.452	61.9	295
9	1.67	.81	1.59	54.4	67.6

TABLE V

Data for Aluminum-Copper Heats -- Non-Plane Front
Solidification

HEAT NUMBER	C_0 (wt.%)	C_s (wt.%)	$u \times 10^3$ (cm/sec)	G_s ($^{\circ}\text{C./cm}$)	$\frac{G_s}{c_s} \left(\frac{^{\circ}\text{C.}}{\text{cm-wt.}\%} \right)$
19	4.32	2.81	1.62	72.1	32.0
20	3.64	2.18	1.87	72.9	33.5
21	1.84	1.02	1.97	69.7	68.4
22	2.84	1.79	1.52	68.2	38.1
23	1.43	1.00	3.18	56.4	56.4
24	9.90	5.32	1.59	57.9	10.9

TABLE VI

Data for Aluminum-Zinc Heats -- Plane Front Solidification

HEAT NUMBER	C_0 (wt.%)	C_S (wt.%)	$u \times 10^3$ (cm/sec)	G_S ($^{\circ}\text{C.}/\text{cm}$)	$\frac{G_S}{c_S} \left(\frac{^{\circ}\text{C.}}{\text{cm-wt.}\%} \right)$
10	1.98	1.35	4.15	71.6	53
11	4.00	3.01	10.0	68.2	22.6
12	5.33	3.20	9.56	60.4	19.1
13	6.99	5.41	16.3	62.6	11.6
14	1.03	6.65	20.5	64.2	9.6
15	5.18	3.93	21.8	64.3	16.5
16	5.42	2.91	2.81	61.1	21.0
17	5.23	3.30	5.52	59.5	18.0
18	8.86	4.75	9.35	58.6	12.4

TABLE VII

Data for Aluminum-Zinc Heats -- Non-Plane Front
Solidification

HEAT NUMBER	C_0 (wt.%)	C_S (wt.%)	$u \times 10^3$ (cm/sec)	G_S (°C./cm)	$\frac{G_S}{c_S} \left(\frac{°C.}{cm-wt.\%} \right)$
25	20.25	14.13	.776	63.9	4.53
26	29.50	19.95	1.14	67.4	3.38
27	16.10	11.54	1.37	64.6	5.6
28	9.86	7.72	2.82	65.9	8.55
29	48.35	32.86	.945	71.0	2.16

APPENDIX A

The relationship between the temperature gradient in the liquid at the interface G , and the temperature gradient in the solid, G_s , may be derived as follows. The total heat flow through the solid plug may be written:

$$k_s A G_s = k_l A G + \Delta H_f \rho A u$$

or

$$G = \frac{k_s G_s - \Delta H_f \rho u}{k_l}$$

For the power inputs and rates of solidification used throughout this work, the heat of fusion term in the above numerator is completely negligible. The expression above then reduces to:

$$G = \frac{k_s G_s}{k_l}$$

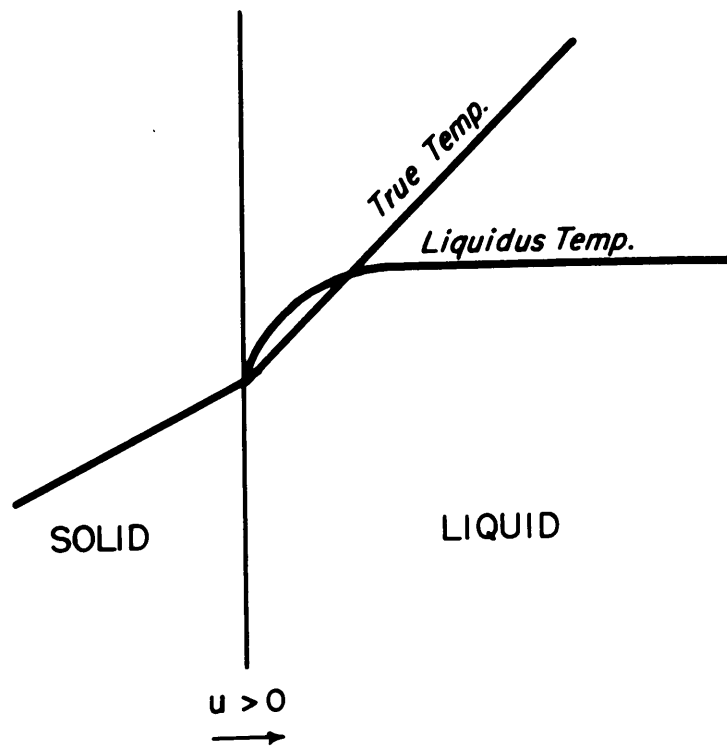


Figure 1 - A Schematic Representation of "Constitutional Supercooling"

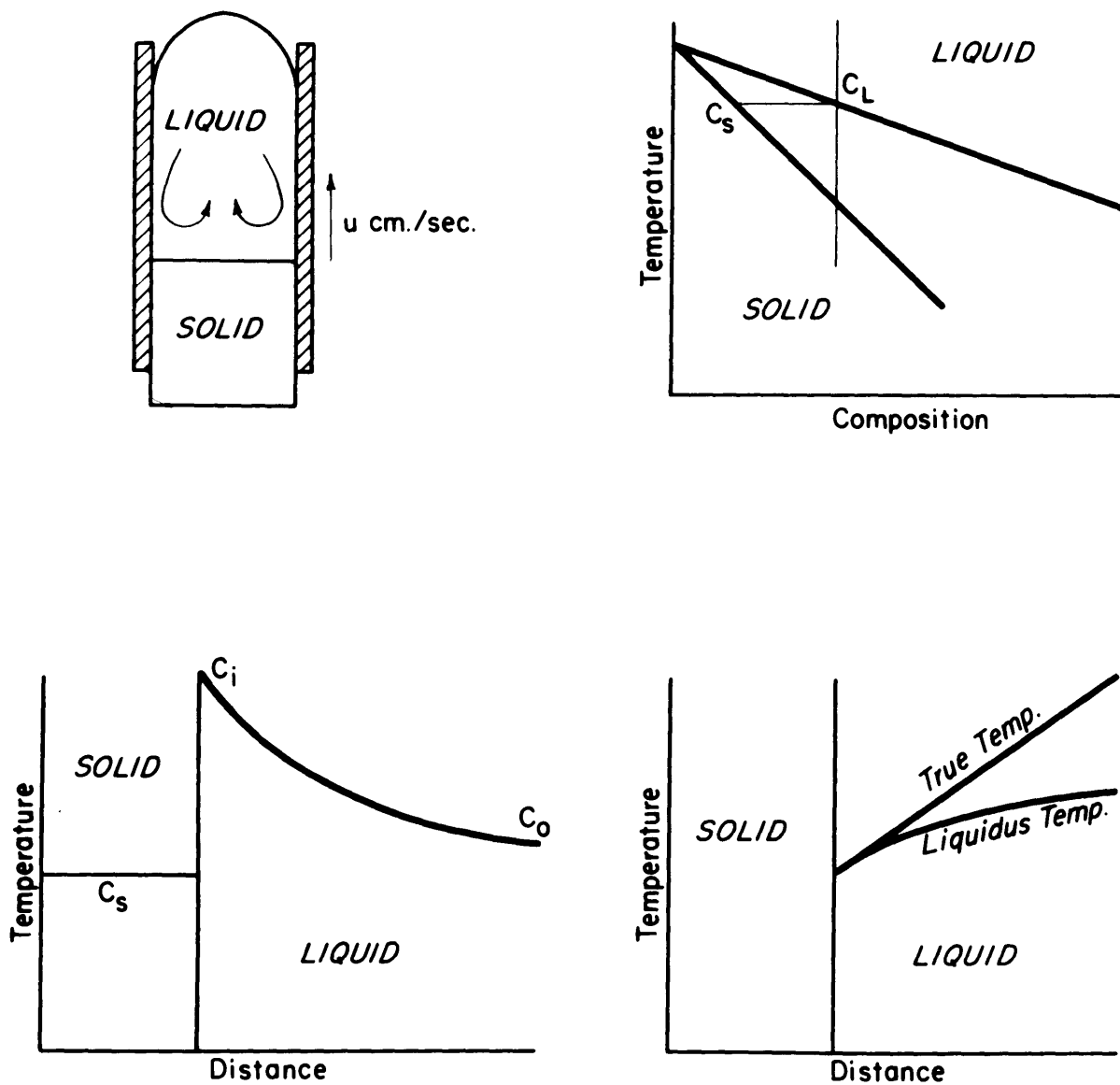


Figure 2 - General Scheme of the Experimental Apparatus Used

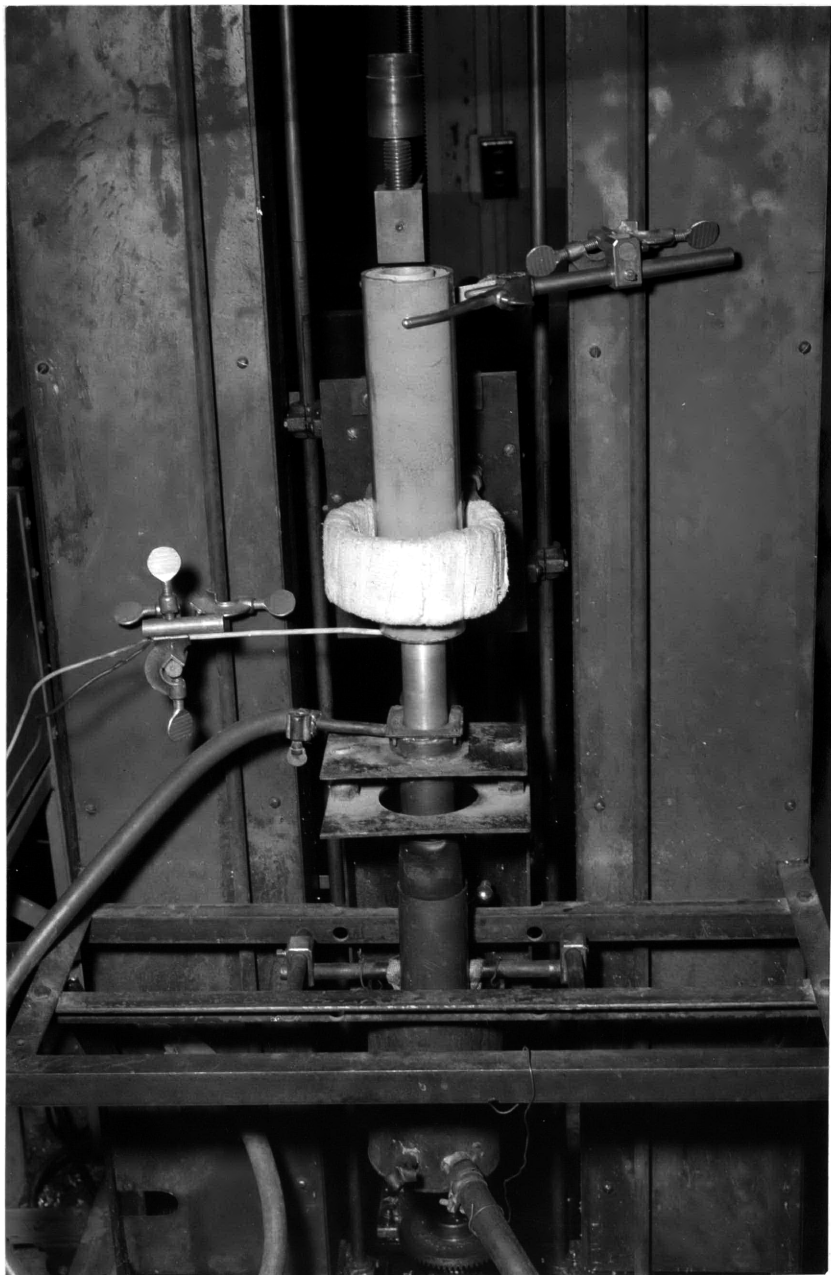


Figure 3 -- Photograph of Crucible and Cooling
Assembly

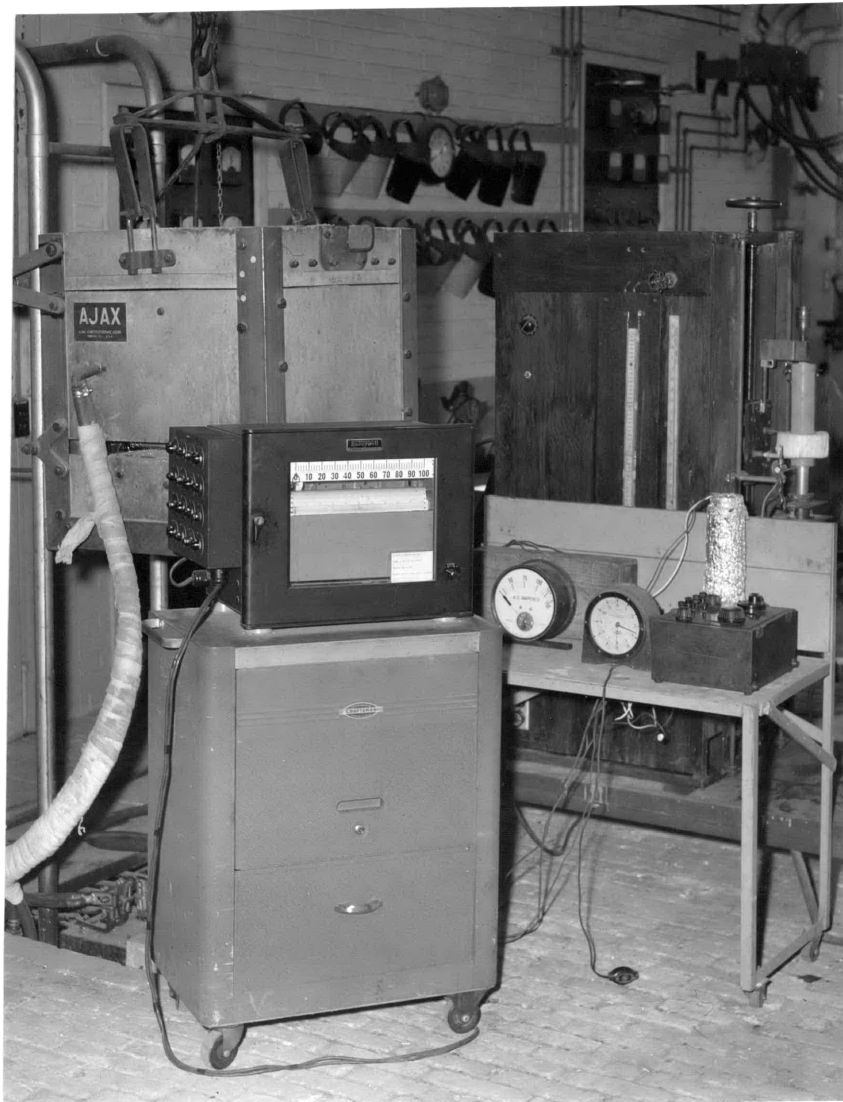


Figure 4 -- Photograph of Experimental Apparatus

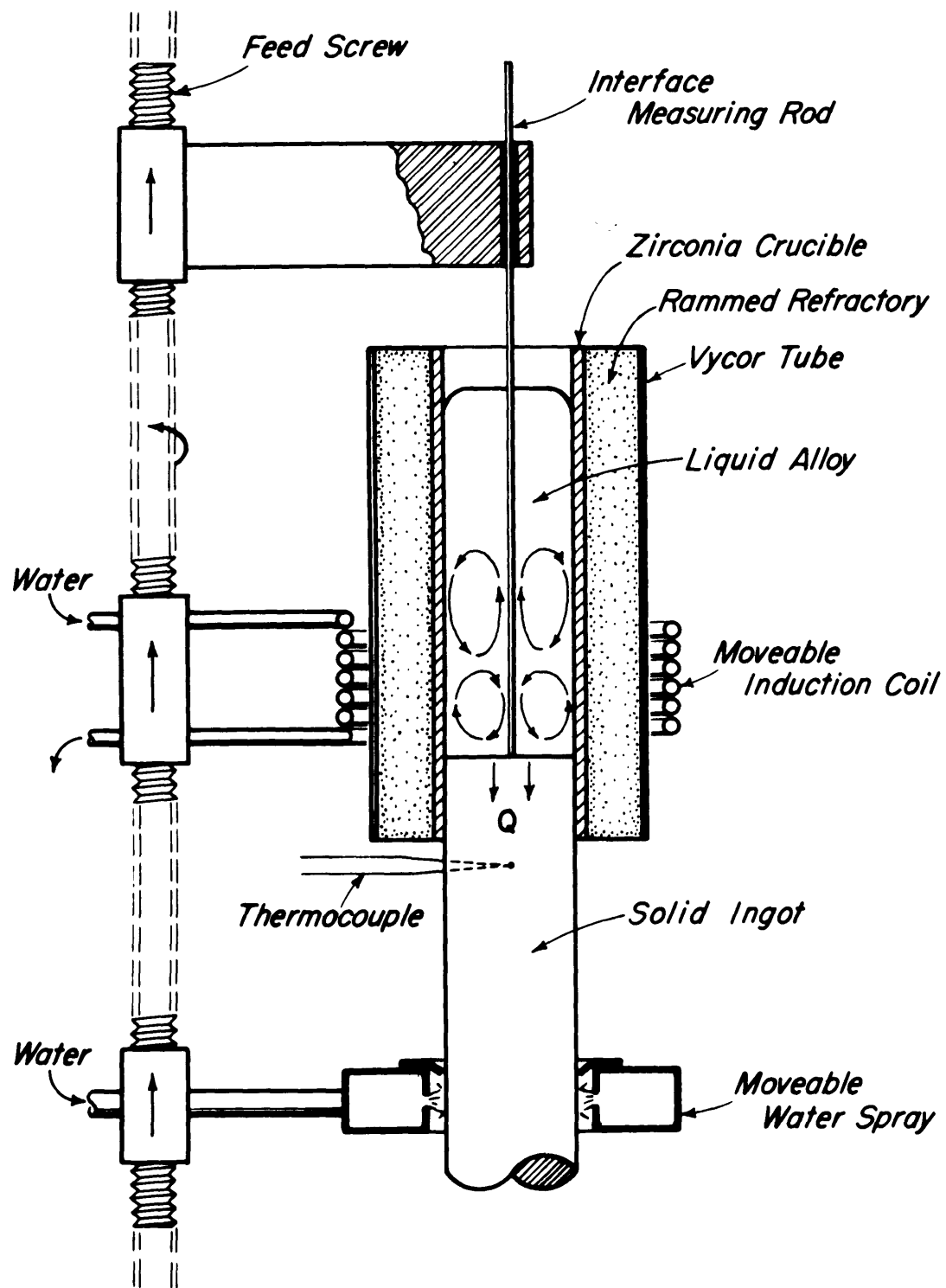


Figure 5 - Diagram of the Basic Elements of the Apparatus

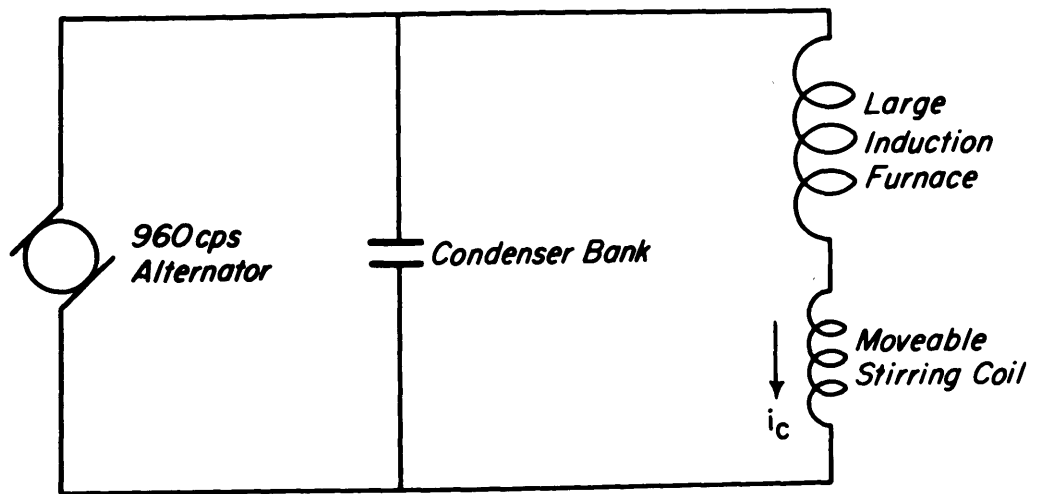


Figure 6 - Overall Schematic Circuit Diagram

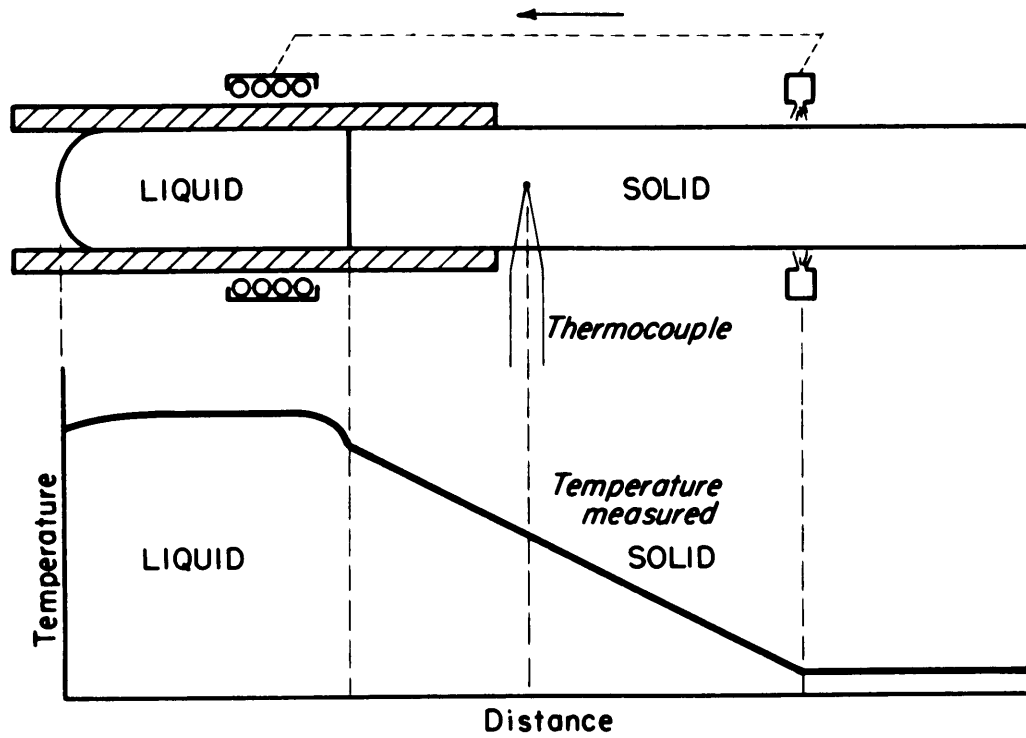


Figure 7 - Schematic Representation of the Steady State Temperature Distribution

PURE ALUMINUM
MELT-DOWN AT CONSTANT POWER
COIL AND WATER STATIONARY

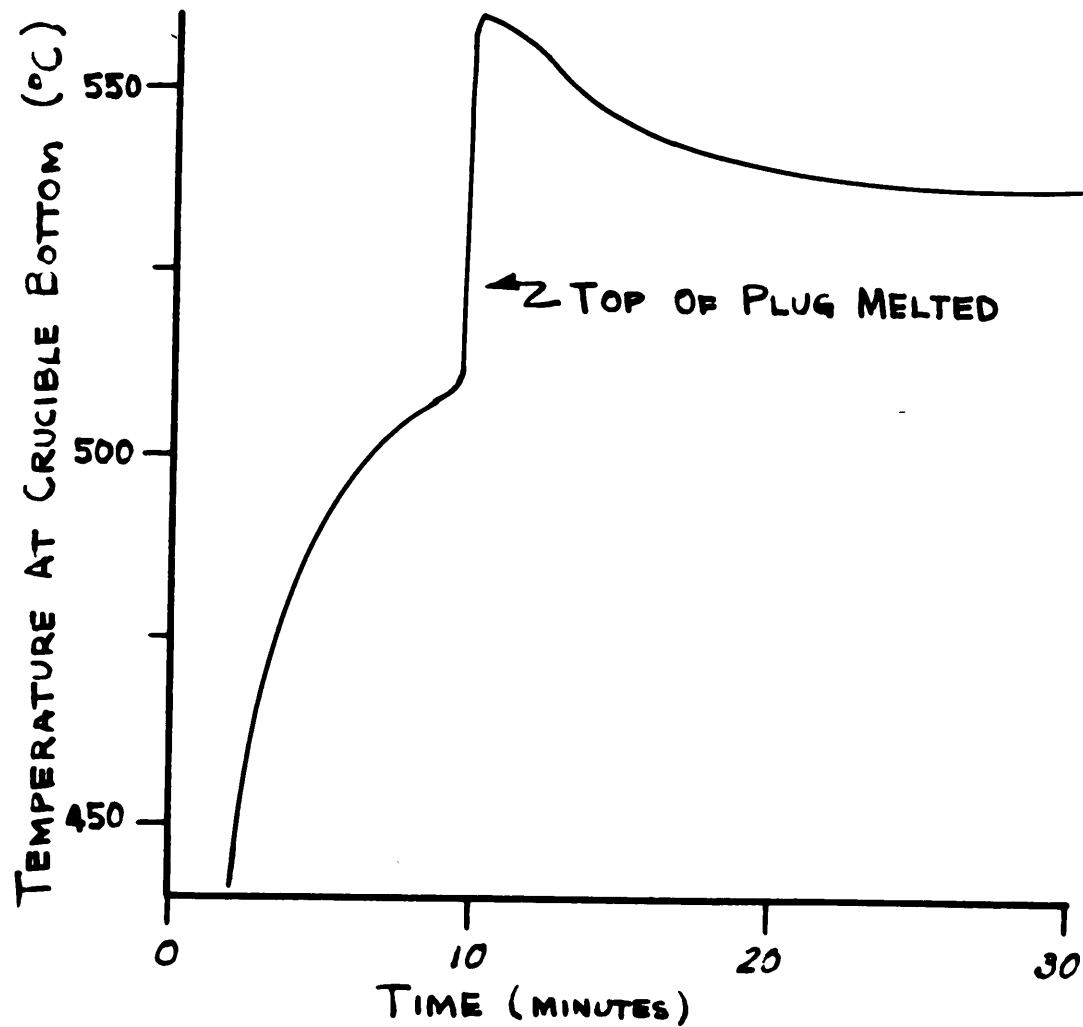


Figure 8 - A Plot of Measured Plug Temperature versus Time Showing the Effect of Ingot-Plug Contact Resistance

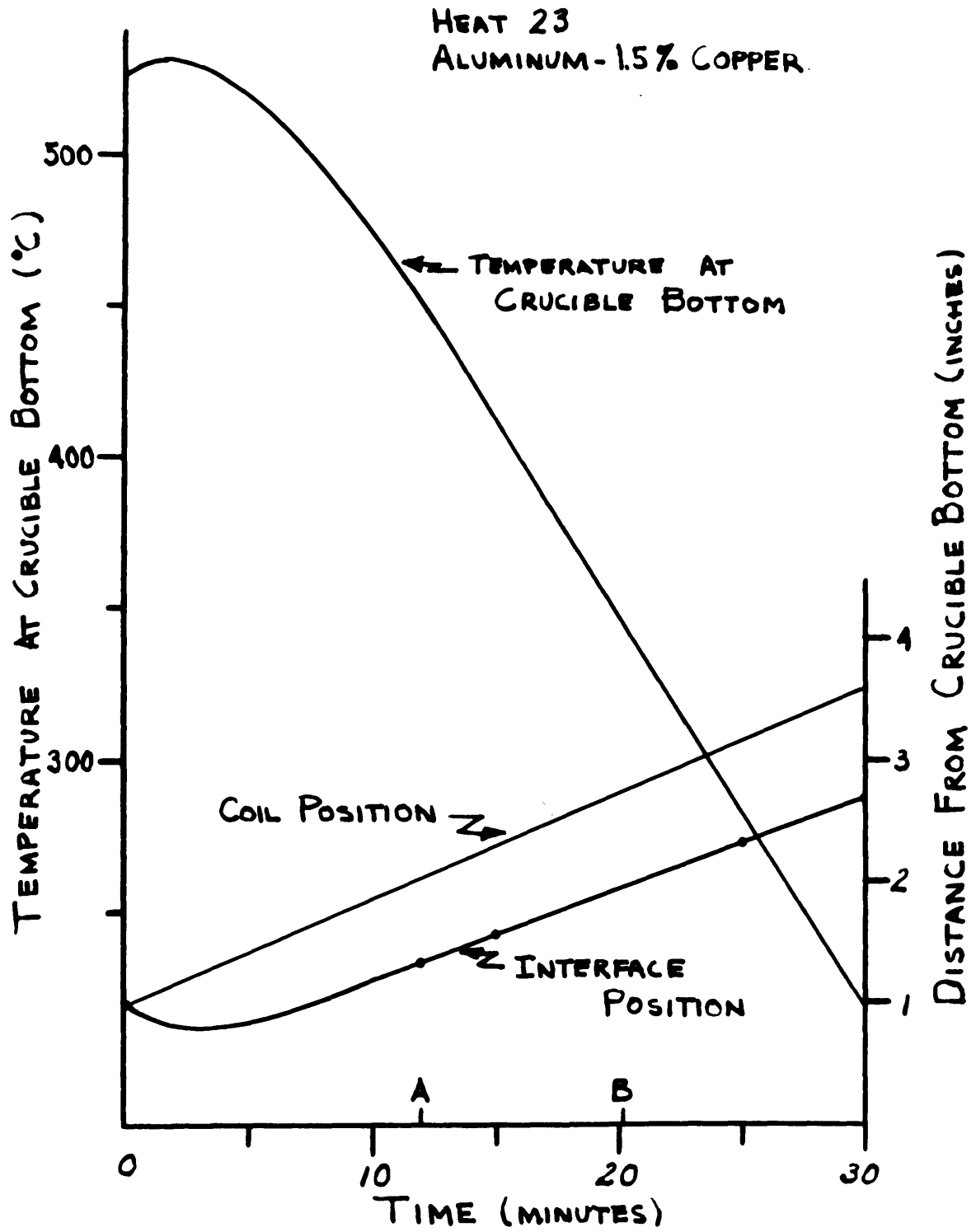


Figure 9 - An Experimental Plot for a Typical Heat

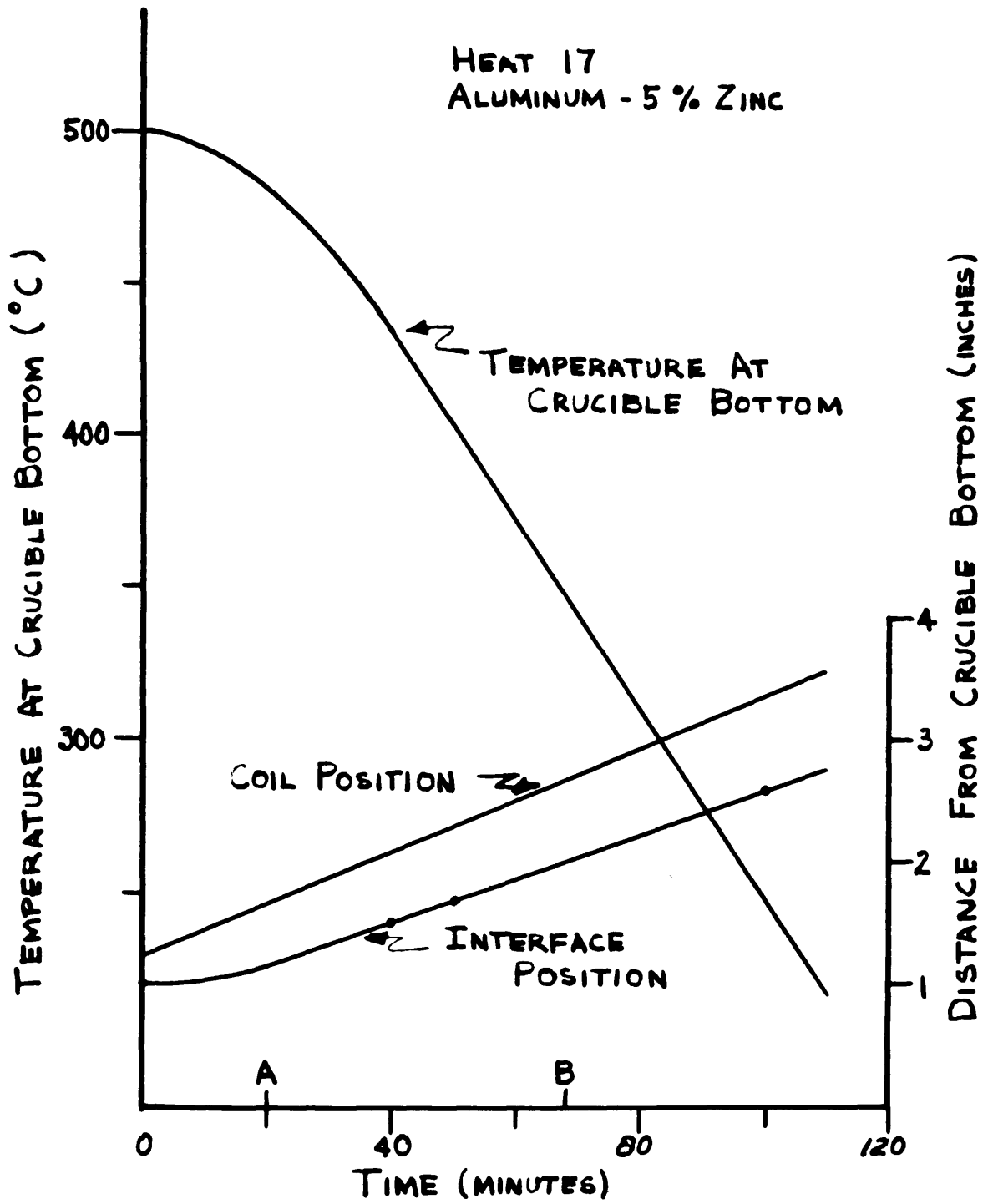


Figure 10 - An Experimental Plot for a Typical Heat

HEAT 23
ALUMINUM - 1.5 % COPPER

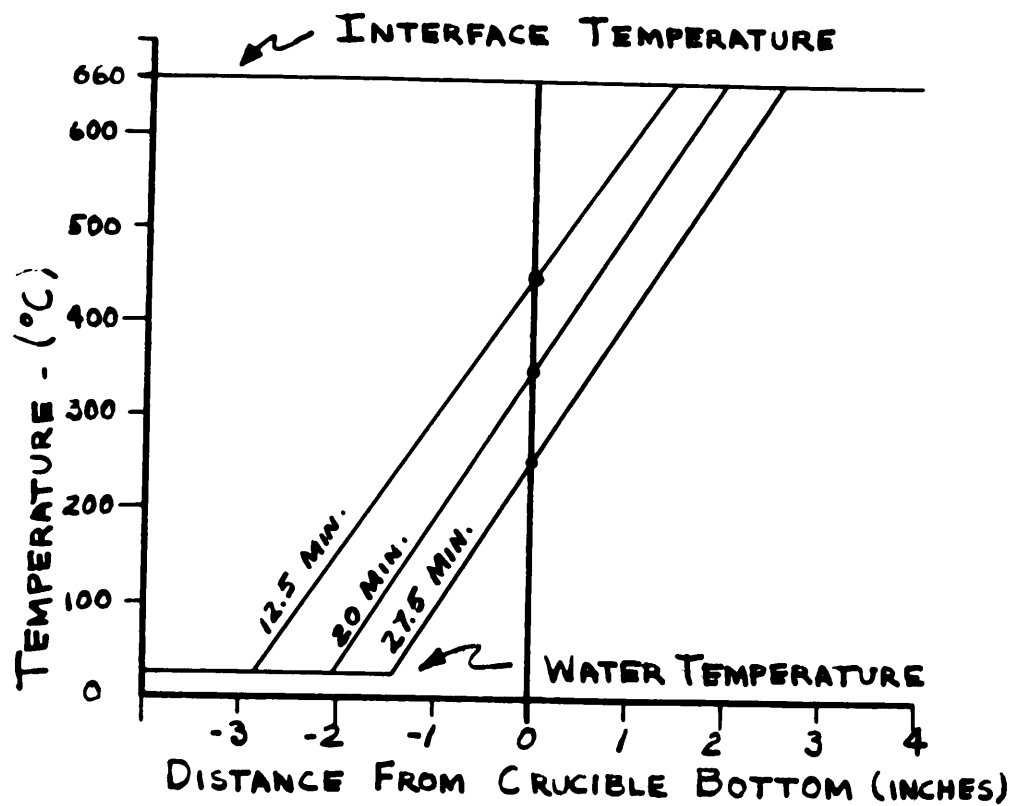


Figure 11 - A Plot Showing Temperature Gradients in the Cooling Plug at Various Times during a Heat.

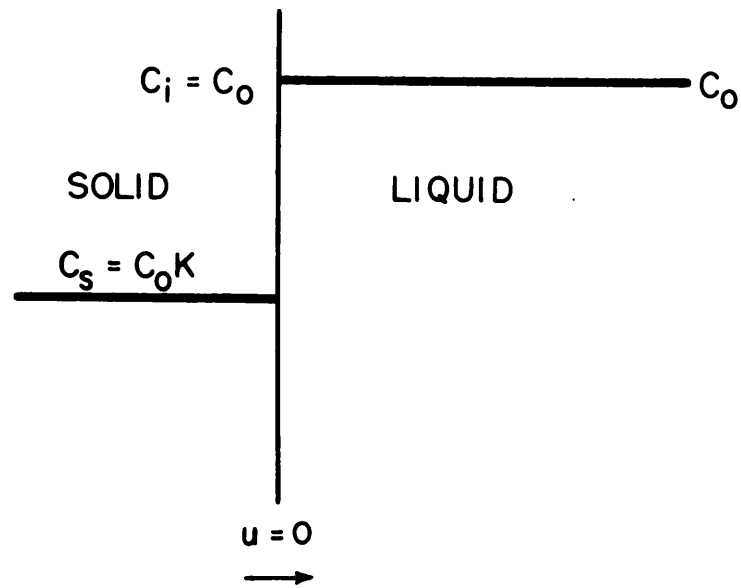


Figure 12 - Composition Gradients at Equilibrium with a Stationary Interface.

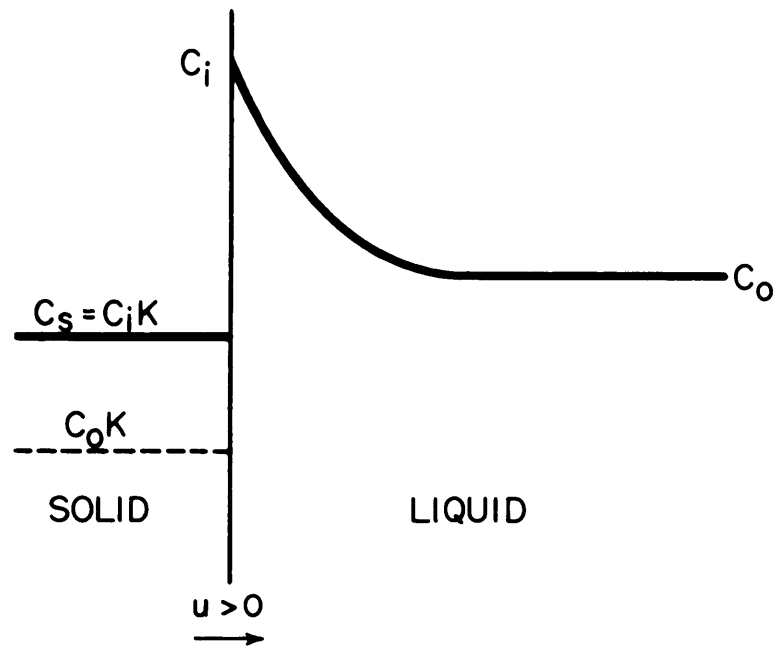


Figure 13 - Composition Gradient with a Moving Interface.

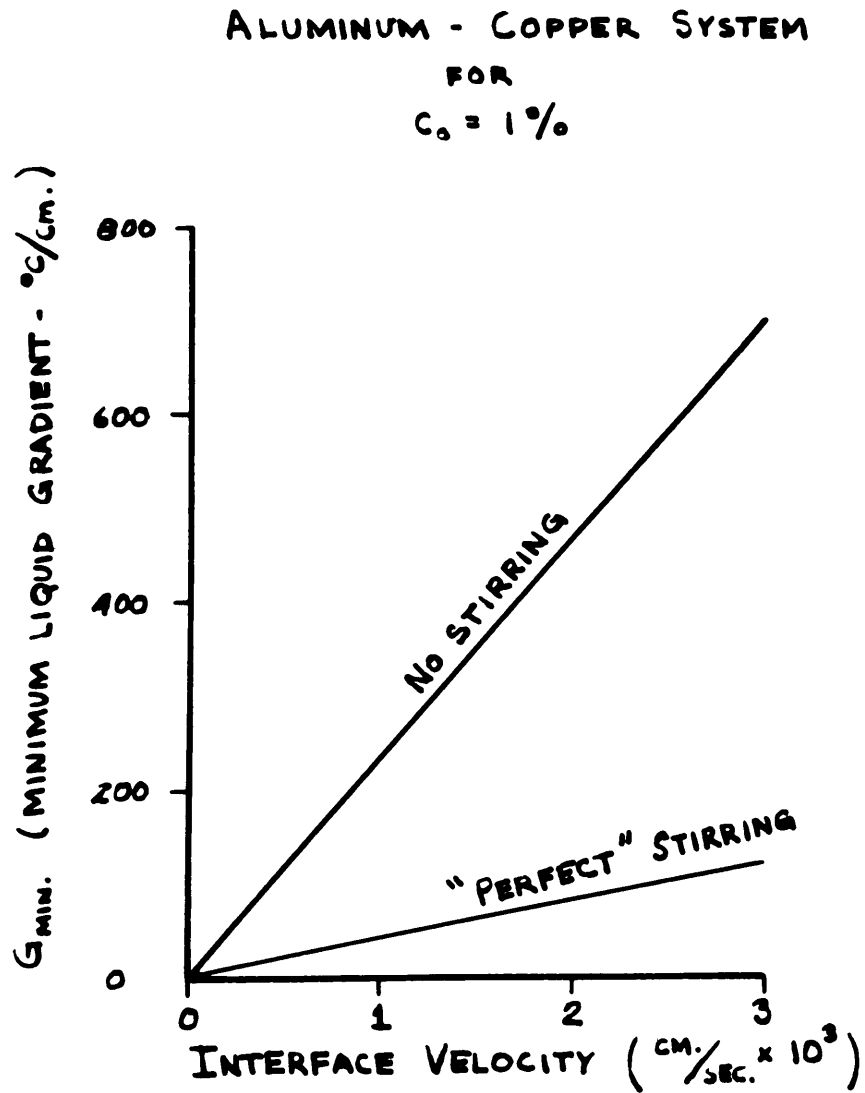


Figure 14 - A Plot of Required Liquid Temperature Gradient versus Interface Velocity for the Aluminum-Copper System

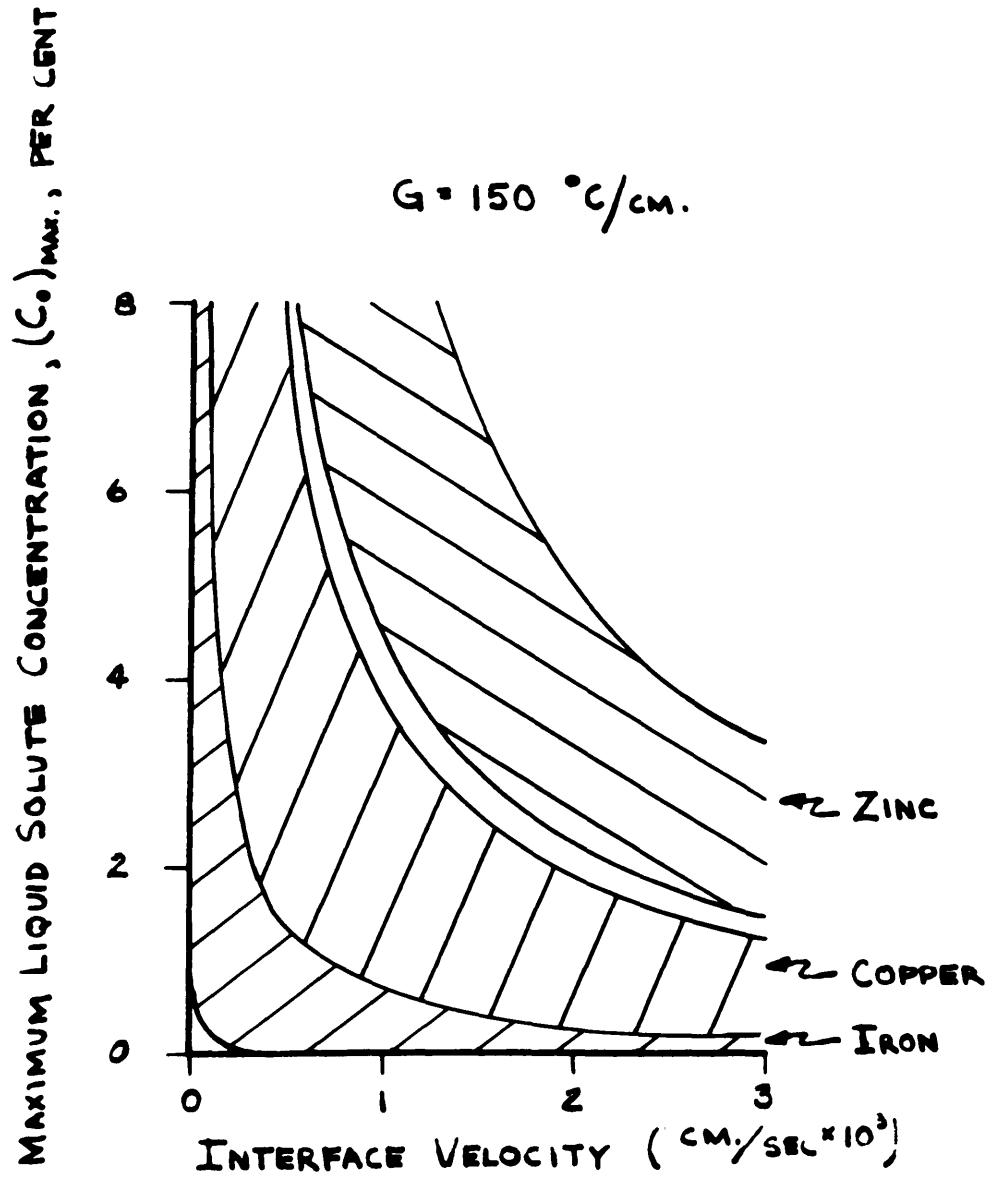


Figure 15 - Plot of Maximum Allowable Concentration, Versus Interface Velocity for Three Different Solutes in Aluminum



Figure 16 -- Macrostructure of Heat 7



Figure 17 -- Macrostructure of Heat 21

Figure 19 -- Microstructure at the Top of the Controlled Solidification Zone of Heat 3. 100X

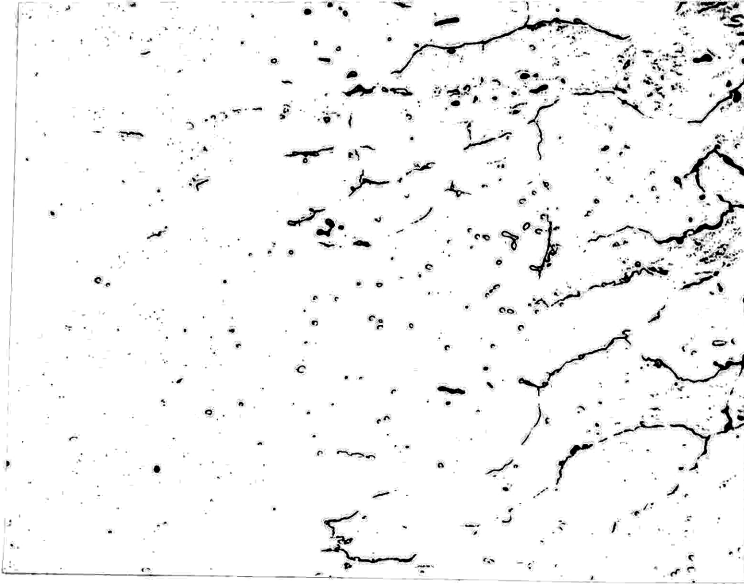
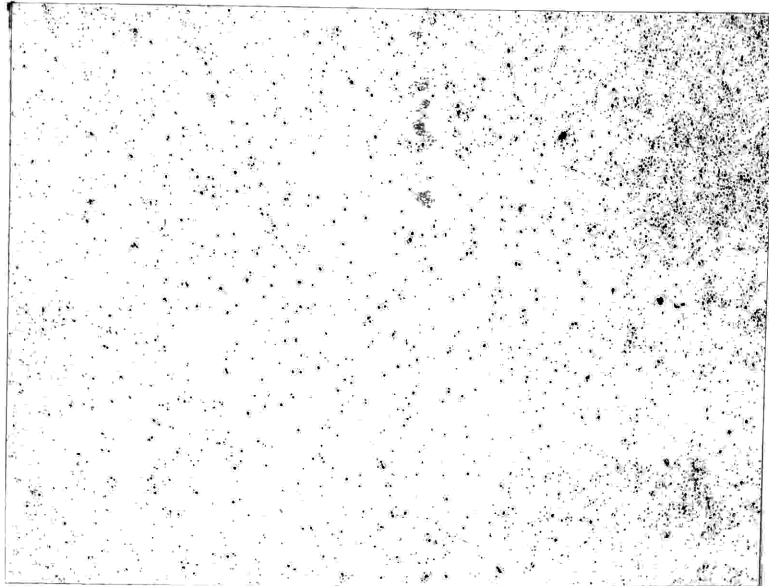


Figure 18 -- Microstructure of Heat 3. 100X



comparable?

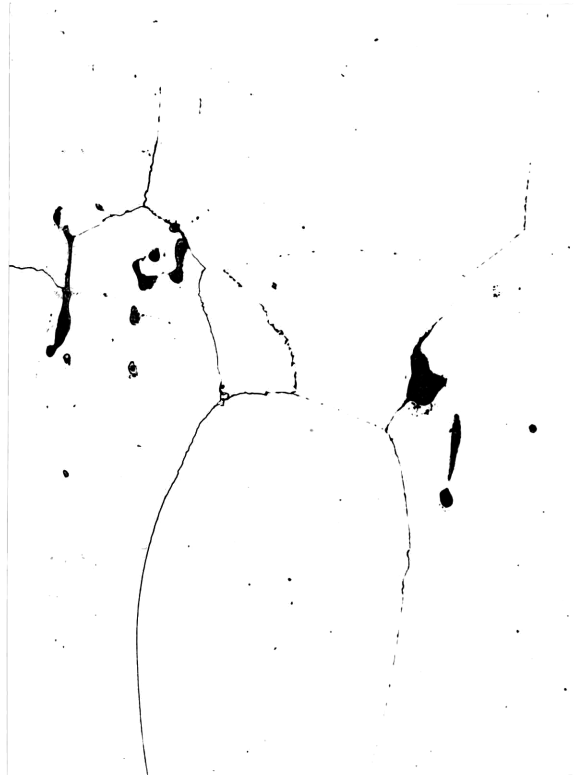


Figure 20 -- Microstructure of Heat 19.
100x

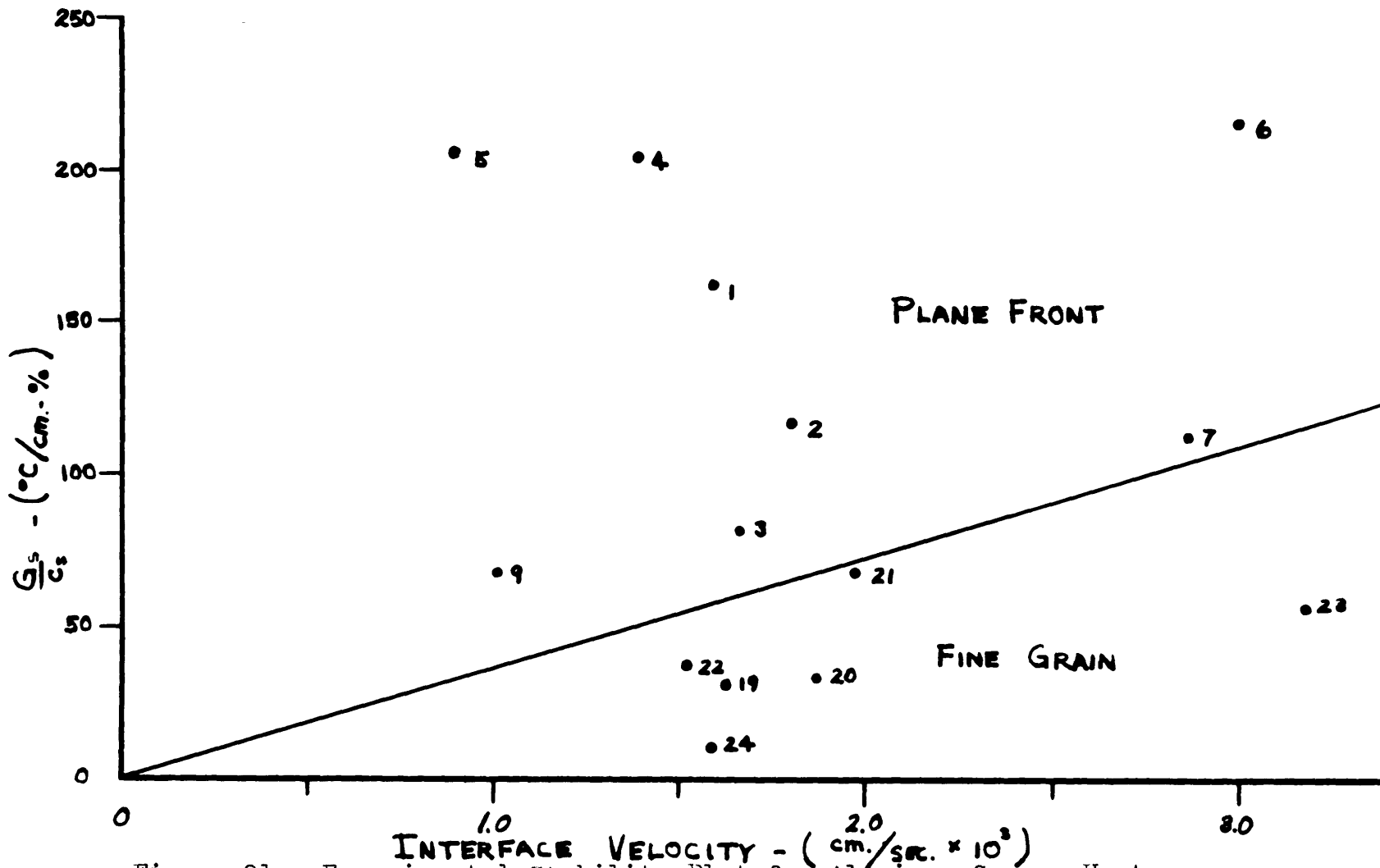


Figure 21 - Experimental Stability Plot for Aluminum-Copper Heats

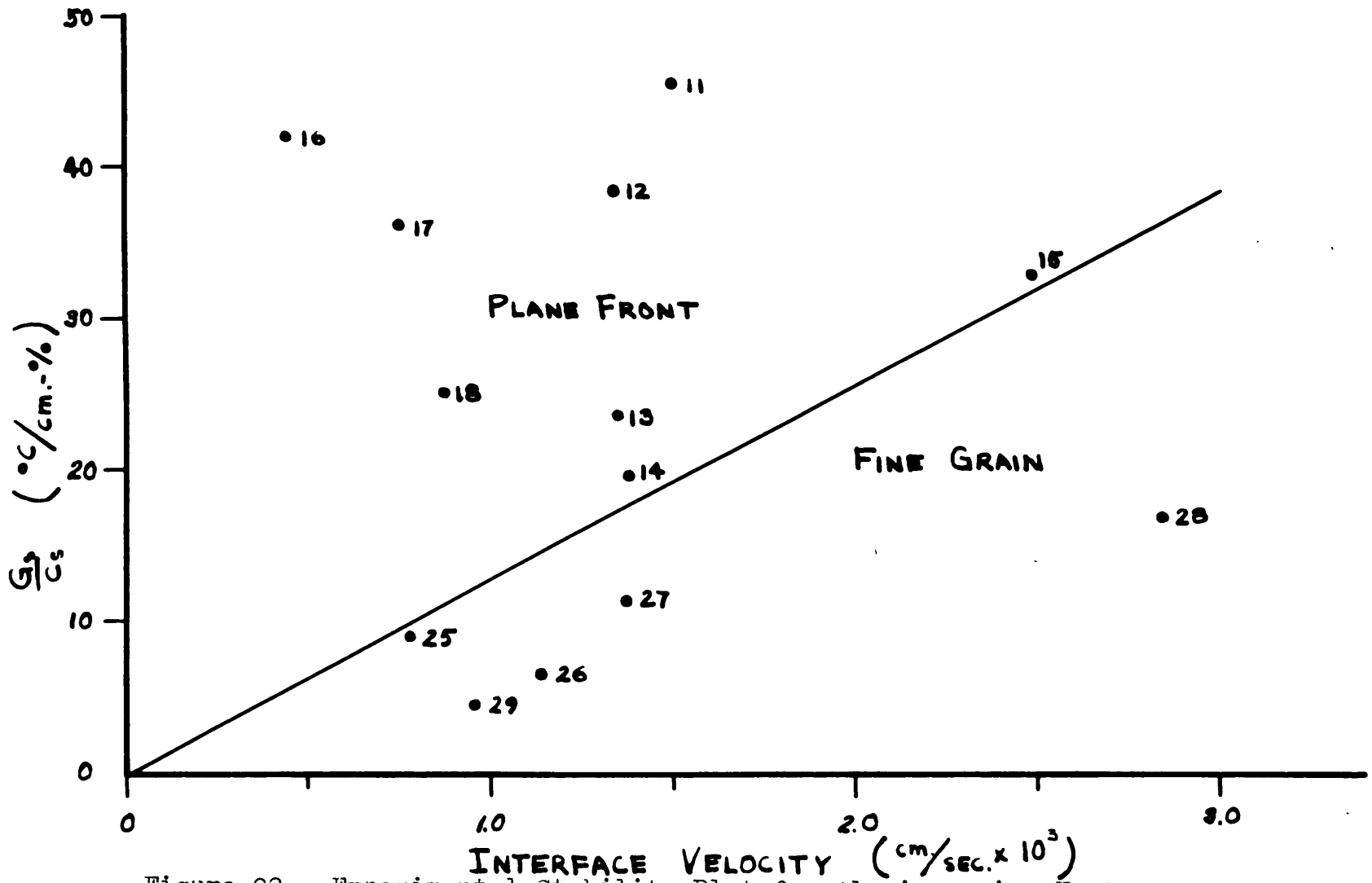


Figure 22 - Experimental Stability Plot for Aluminum-Zinc Heats



Figure 23 -- Macrostructure of Heat 15



Figure 24 -- Macrostructure of Heat 25



Figure 25 -- Macrostructure of Heat 33



Figure 26 -- Macrostructure of Heat 34



Figure 27 -- Macrostructure of Heat 20

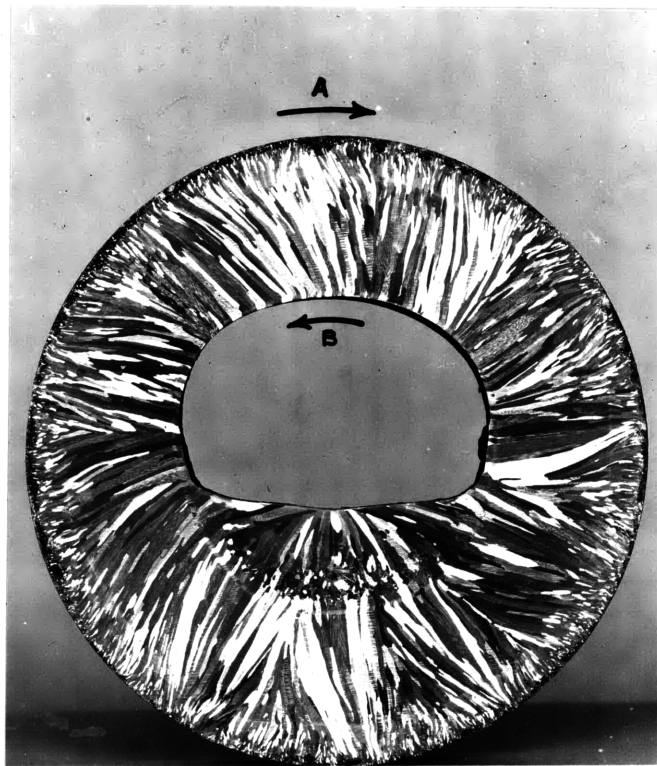


Figure 28 -- Structure of a Copper
Centrifugal Casting